Broadband and Low-Frequency Acoustic Liner Investigations at NASA and ONERA

Michael Jones, Frank Simon, Rémi Roncen

Broadband and Low-Frequency Acoustic Liner Investigations at NASA and ONERA

Michael G. Jones*

NASA Langley Research Center, Hampton, VA 23681

and

Frank Simon†, Rémi Roncen†

ONERA/Département Multi-Physique pour l'Énergétique,

Université de Toulouse, F-31055, Toulouse, France

NASA and ONERA have explored a number of acoustic liner concepts over the last few decades. This paper begins with a brief review regarding conventional liners as well as the recent implementation of multi-degree-of-freedom liners enabled by embedded mesh caps. Six novel liner concepts are presented, along with the accompanying impedance prediction models used in their design. Each of the NASA concepts is designed to vary the impedance over the surface of the liner in a controlled manner, whereas the ONERA concepts make use of long neck acoustic resonators. Selected results are presented for each of these liners evaluated in the NASA and ONERA test rigs. Finally, a set of aeroacoustic metrics is defined for comparison standardization between conventional and innovative acoustic liners and all the concepts are compared on this basis.

Nomenclature

Symbols	Description
a	semiempirical constant used in the Motsinger Kraft Model (MKM)
A, B	parameters used in the MKM for DC flow resistance

*Structural Acoustics Branch, AIAA Associate Fellow, michael.g.jones@nasa.gov (Corresponding author).
†Aerodynamics and Energetics Modeling Department, ONERA Midi-Pyrenees Toulouse Center.

Symbols	Description
$b, b^{'}$	intermediate parameters [Eq. (19)]
$c_0, \tilde{c}_{eq}$	local sound speed of air, equivalent sound speed
C_D	discharge coefficient
C_p, C_v	specific heat of air at constant pressure, specific heat of air at constant volume
d, d_c, d_p	facesheet hole diameter, chamber diameter, penetration depth
f	frequency
h	chamber height
i	imaginary unit, $\mathrm{i} = \sqrt{-1}$
J_0, J_2	Bessel functions of the first kind with orders 0 and 2
$k, \bar{k}, \tilde{k}_{eq}$	freespace wavenumber, reduced frequency, equivalent wavenumber
$\widetilde{K}_{eq}, K_0$	equivalent complex bulk modulus of fluid, intermediate parameter
l_t	material thickness of hollow tube (LEONAR concept)
LFP	low-frequency performance
M	mean flow Mach number
M_p	maximum peak value of absorption coefficient within bandwidth
$N, N^{'}$	intermediate parameters [Eq. (18)]
N_{ch}, N_p	number of chambers in liner, number of facesheet perforates per chamber
n_Γ	intermediate parameter [Eq. (7)]
p, P_{ref}, P_0	acoustic pressure, reference pressure (20 μPa), atmospheric pressure
p_0, p_1, p_2, p_3, p_4	acoustic pressures at planes 0 through 4 (Sec. IV)
Pr	Prandtl number
r	perforation radius
R, R_f	reflection coefficient, DC (steady) flow resistance
s	shear wave number
S_{ch}, S_p	cross-sectional areas of chamber and perforate
t	material thickness
$T_{11}, T_{12}, T_{21}, T_{22}$	transfer matrix coefficients

Symbols	Description
T_{es}	transfer matrix for equivalent fluid layer with a semiphenomenological modeling of porous media
u, V	acoustic particle velocity, mean velocity
u_0, u_1, u_2, u_3, u_4	acoustic particle velocities at planes 0 through 4 (Sec. IV)
α	absorption coefficient
$\widetilde{\alpha}_{p,i}, \alpha_\infty, \alpha_0, \alpha_0^{'}$	dynamic tortuosity of material in contact with i^{th} side of the perforations, tortuosity, static viscous tortuosity, static thermal tortuosity
β_{ch}, β	admittances of individual chamber and homogenized across the liner surface
β_f, β_1	lowest continuous frequency bandwidth where the absorption coefficient is above a selected threshold, lower bound of the frequency bandwidth
γ_0, Γ	specific heat ratio, propagation constant
δ_1	boundary layer displacement thickness
ϵ_e	static correction associated with interactions between perforations
ϵd	end correction in facesheet mass reactance
$\zeta_c, \zeta_s, \tilde{\zeta}_{eq}$	characteristic impedance, normalized surface impedance of liner, equivalent impedance
θ, χ	normalized resistance, normalized reactance
κ_i, κ_e	empirical constants that account for entrance and exit end effects
κ_0, κ_0'	static viscous permeability, static thermal conductivity
λ	acoustic wavelength
$\Lambda, \Lambda^{'}$	viscous characteristic length, thermal characteristic length
μ, ν_0	coefficient of dynamic viscosity, kinematic viscosity
$\rho_0, \rho_s, \widetilde{\rho}_{eq}$	local density, static density, equivalent complex fluid density
σ_0	static (Darcy) flow resistivity
ϕ	material volume porosity
ω, ω_c	angular frequency, JCAPL angular frequency
$\omega_c^{'}$	intermediate parameter [(Eq. 18)]
Ω	surface open area ratio

Symbols	**Description**

Abbreviations	**Description**
BPF	blade passing frequency
DC	direct current (herein related to the steady component of flow resistance)
GFIT	grazing flow impedance tube
JCA, JCAPL	Johnson-Champoux-Allard and Johnson-Champoux-Allard-Pride-Lafarge models
LEONAR	long elastic open neck acoustic resonator
MKM	Motsinger Kraft Model
SDOF, 2DOF, MDOF	single-, two-, and multi-degree-of-freedom
SPL	sound pressure level
ZKTL	Zwikker and Kosten transmission line model

Subscripts	**Description**
C/L	centerline
fs	facesheet
gf	grazing (tangential) flow
inc	incident
N	normal
p, i	sides '1' and '2' of perforation
rms	root mean squared

I. Introduction

Acoustic liners are passive devices that are typically mounted in the walls of aircraft inlets and aft-bypass ducts (see Fig. 1) to absorb noise generated by the fan. These liners have been almost exclusively limited to single-degree-of-freedom (SDOF) or two-degree-of-freedom (2DOF) perforate-over-honeycomb structures (see Fig. 2) since the early 1950s.[1] However, there has been a strong trend toward engines with higher bypass ratios over the last few decades, with a resultant need for larger diameter fans. To keep the weight down, and thereby to constrain fuel costs, engine manufacturers have also sought to reduce the length of

engine nacelles.

These nacelle geometry changes have had a number of effects on the signature of noise generated by the engine and on the effectiveness of the acoustic liners. Whereas fan and jet noise were both major components of noise produced by lower bypass ratio fans, significant increases in bypass ratio have caused jet noise to be greatly reduced but have had no such benefit for the fan noise component.

The blade passing frequency (BPF) of the fan is a major contributor to the tonal component of fan noise. Since the BPF is inversely proportional to the diameter of the fan and the maximum blade tip Mach number is prescribed, acoustic liners must be tuned to achieve peak noise attenuation at lower frequencies (e.g., down to approximately 500 Hz) in order to accomodate increases in fan diameter. Typically, the thickness of the liner would need to increase to achieve attenuation at lower frequencies. However, thicker liners would increase the weight of the engine (and therefore, the amount of fuel required), which is undesirable.

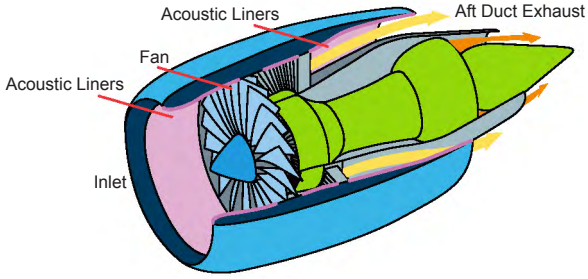

Figure 1: Cutaway sketch of generic aircraft engine nacelle.

(a) SDOF. (b) 2DOF.

Figure 2: Sketches of SDOF and 2DOF acoustic liners.

The increase in bypass ratio has also changed the fan noise spectrum. This spectrum was dominated by tonal content (rotor-alone and rotor-stator interaction) for low bypass ratio fans, but now contains much

more broadband (noise generated by turbulent mean flow through the nacelle) content. In addition, the simultaneous increase in fan diameter and decrease in nacelle length causes the effectiveness of existing acoustic liners to be reduced. Nevertheless, the International Civil Aviation Organization and the Federal Aviation Administration continue to require further noise reduction to allow for continued growth of the commercial aircraft fleet without negatively impacting the communities surrounding airports.[2] As a result, there is a need for acoustic liner concepts that (1) achieve more noise attenuation in spite of the decrease in length-to-duct height ratio, (2) require less surface area to fit within shorter nacelles, (3) require less liner thickness to reduce total weight (hence, fuel consumption), and (4) extend attenuation to lower frequencies to account for lower blade passing frequencies.

A plethora of liner concepts have been proposed over the last two decades. While it is impossible to do justice to the vast array of concepts, the following sampling is intended to demonstrate the wide-ranging approaches that have been considered. Many concepts have targeted low-frequency sound absorption. Two of these include Herschel-Quincke tube liners[3] and 3D folded-core acoustic liners.[4] Other concepts have targeted broadband sound absorption, such as checkerboard liners,[5] dual-resonance liners,[6] and liners that incorporate flexible walls within the liner core.[7]

Many concepts have employed features to adaptively modify the impedance to enable in situ tuning of the sound absorption frequency range. For example, Bielak et al.[8] used bias flow and temperature control to modify the sound field within the liner, whereas Bake and Knobloch[7] achieved similar results by embedding a loudspeaker within an SDOF liner (hybrid zero massflow liner). Shape memory alloys[9] and tunable electromechanical Helmholtz resonators[10] have been used as adaptive techniques for in situ impedance control, and Ichihashi[11] describes an acoustic structure for which the open area through the septum can be varied via flappers.

There has also been increased interest in the application of acoustic liners in unconventional locations. A number of these applications have been explored by NASA and ONERA (e.g., anti-icing liners, soft vanes, treated bifurcations, over-the-rotor liners, liners on surface of wing or fuselage, flap side-edge liners, landing gear door and bay liners, air conditioning systems, wind tunnel heated duct for nozzle modeling, anechoic wind tunnel).[12–19] Fortunately, there has been much progress in the areas of manufacturing, especially in additive manufacturing (3D printing). As a result, it has become much easier to evaluate new concepts and determine whether they are suitable for more thorough study.

The potential to use acoustic liners in novel locations introduces additional restrictions. Many of these applications require the acoustic treatment to be placed in small locations (e.g., within a fan exit guide vane; soft vane). Therefore, many concepts are designed for the express purpose of packaging a liner into a small space.[20, 21] Replacing a smooth, solid surface with an acoustic liner causes the aerodynamic drag to

increase due to the roughness of the facesheet perforations and the acoustically forced flow through acoustic liners. Given the critical need for noise reduction in commercial aircraft engine nacelles, the benefits of noise reduction outweigh the concerns of additional drag caused by liners mounted in traditional locations within the nacelle (otherwise, current aircraft would not include liners). Similarly, it must be demonstrated that the placement of acoustic liners in nontraditional locations results in a sufficient reduction in noise to outweigh the concerns of additional drag. Although it has been demonstrated that modification of the geometry of facesheet perforations can be employed to reduce this liner drag,[22] further drag reductions are needed. In summary, the designer is always faced with the need for compromise between noise and fuel consumption concerns.

The purpose of this article is to review some of the novel acoustic liner concepts that have been investigated by NASA and ONERA. Each of the NASA concepts uses a variable surface impedance to achieve broadband sound absorption, while each of the ONERA concepts uses the LEONAR (long elastic open neck acoustic resonator) approach to provide broadband sound absorption centered on a lower frequency. The predicted and measured results presented herein target a no-flow environment, but the effects of grazing flow on acoustic liners are very important for application in aircraft engine nacelles. Thus, the effects of grazing flow are briefly addressed as well.

Section II provides a description of conventional liners with some of their limitations. This description is needed as a guide for development of additional liner concepts. Section III provides a description of design targets for liners and analytical and experimental tools used in the development and evaluation of these liner concepts are presented in Sections IV and V. Section VI presents a discussion of recent novel liner concepts investigated at NASA and ONERA, and Section VII provides a discussion of metrics proposed for comparison of liner concepts. Section VIII closes with some concluding remarks.

II. Review of Conventional Liners

This section begins with a brief discussion of acoustic impedance, generally accepted as the key parameter for acoustic assessment of a liner. This is followed by a brief review of SDOF and 2DOF conventional acoustic liners that have been widely used for many years. Finally, some recent additional flightworthy options are presented that provide sound absorption over a wider frequency range.

A. Acoustic Impedance

Acoustic impedance, ζ_s, is defined as the ratio of the Fourier transforms of the acoustic pressure and the normal component of acoustic particle velocity at a point of interest (e.g., at the surface of the liner),[23]

and is commonly represented as

$$\zeta_s = \frac{p}{\rho_0 c_0 u_N} = \theta + \mathrm{i}\,\chi. \tag{1}$$

This impedance (assumed normalized by the characteristic impedance of air, $\rho_0 c_0$, where ρ_0 and c_0 represent the local density and sound speed of air, respectively) is a function of frequency, the liner geometry, and the aeroacoustic environment where the liner is placed. The real and imaginary components of impedance are labeled the resistance, θ, and reactance, χ, respectively. Acoustic resistance is a measure of the forces (e.g., viscous losses) that dissipate the acoustic energy (e.g., convert it to heat), whereas acoustic reactance determines the frequencies where this energy conversion process is optimal (where χ approaches zero). The acoustic impedance is an intrinsic property of an acoustic liner, which implies it is independent of duct geometry. This is critical to the liner designer, as it indicates a detailed study in a controlled environment can be used to properly evaluate a liner, and the results can be used to predict the response of that liner in an aircraft engine nacelle.

The liner concepts discussed in this article are intended to present a desired acoustic impedance spectrum, $\zeta_s(f, M, \mathrm{SPL})$, at their surface. It is assumed that aeroacoustic propagation codes can be used to determine the optimum impedance spectrum for a specific application (e.g., treatment placed in the walls of an aircraft inlet). Thus, the goal of the liner designer is to come up with liner configurations that will most closely achieve these desired impedance spectra.

B. Single and Two Degree-of-Freedom Liners

Figure 2 presents liner configurations that are currently employed in aircraft engine nacelles. SDOF liners are often referred to as quarter-wavelength resonators, as their acoustic performance (absorption) is maximized at frequencies for which the wavelength is approximately four times the depth of the core chamber. These passive devices provide significant attenuation at their tuned frequencies (near resonance) and also provide reasonable attenuation for frequencies surrounding this peak frequency. This range of attenuation often extends to about one octave. In 2DOF liners, the addition of a perforated septum to create a second layer causes the liner to absorb sound over a wider frequency range, but tends to reduce the peak attenuation. There are actually three tuning frequencies for a 2DOF liner, one for each of the frequencies with quarter-wavelengths corresponding to the upper, lower, and total core depths. As such, 2DOF liners typically provide improved attenuation over a two-octave frequency range. In summary, SDOF and 2DOF acoustic liners are well established and useful sound absorbers for application to commercial aircraft engine nacelles, especially for lower bypass-ratio engines. However, as noted previously, the continual push toward higher bypass-ratio engines has created a need for improved designs.

C. MDOF Liners Enabled by Embedded Mesh Caps

For decades, the septum in 2DOF liners was a perforated sheet (or wire mesh) that was placed between two disconnected honeycomb core structures. This could result in misalignment between the upper and lower layers, thereby affecting the acoustic performance of the liner. A few options have been employed to overcome this issue. One option employs a mesh-cap manufacturing approach[24] that replaces the embedded perforated sheet with individual sheets of wire mesh placed within each chamber of the core (see Fig. 3) such that the honeycomb material does not need to be cut.

(a) Constant d_p and R_f. (b) Variable d_p and R_f.

Figure 3: Four chambers of a two-layer liner core with embedded mesh caps. Different colors are used to indicate distinct DC flow resistances, R_f, placed at distinct penetration depths, d_p.

If these mesh caps are all identical with uniform penetration depths, the result is a 2DOF liner. However, additional degrees of freedom can be gained by allowing the penetration depths, d_p, and DC flow resistances, R_f, of these mesh caps to vary between adjacent chambers of the core. These additional degrees of freedom allow the designer to extend the frequency range over which sound absorption can be achieved, albeit typically at the expense of slight reductions in peak attenuation. To date, these liners have been designed using modified versions of conventional liner models. However, there is a need for modeling improvements if this concept is to be further optimized.

A number of tests were conducted by NASA[25–30] to explore the feasibility of implementing embedded mesh caps at various technology readiness levels.[31] These tests included two-layer configurations, such as those shown in Figure 3, and three-layer configurations. Perhaps the most significant test to date of this concept was a three-layer configuration (see Fig. 4) that was tested on the inlet of a Boeing B737MAX-7 aircraft. This flight test, labeled the Quiet Technology Demonstrator 3, was a collaboration between NASA and the Boeing Company. The Hexcel Corporation fabricated a three-layer core for the engine nacelle inlet based on a design provided by NASA. The mesh caps for each septum layer were identical (same resistance and pentration depth). The Boeing Company added a perforated facesheet that employed a special perpendicular

slot design that was also provided by NASA, and then installed the resultant liner in the inlet of a Boeing B737MAX-7 aircraft. The flight test (see Fig. 5), conducted in late 2018, demonstrated significant reductions in drag and radiated noise.[32, 33]

(a) Three-layer core. (b) Slotted facesheet.

Figure 4: Components for B737MAX-7 flight test inlet. Photographs provided by the Boeing Company.

Figure 5: B737MAX-7 flight test. Photograph provided by the Boeing Company.

III. Design Goals for Novel Liners

Continual advances in manufacturing techniques and materials enable novel liner configurations. One such advance is in the area of additive manufacturing (3D printing). The speed and relatively low cost associated with additive manufacturing has allowed numerous configurations to be explored by liner designers. As the materials and 3D printers evolve, the possibility of employing complex liner geometries in aircraft applications is becoming a reality. In addition, the use of robotics (e.g., for controlled perforation of solid facesheets installed in a nacelle inlet) within the aircraft manufacturing industry provides additional liner design options.

The initial requirements for novel liners are identical to those for conventional liners. As always, the goal

is to achieve a specified impedance spectrum at the surface of the liner. Ideally, this impedance spectrum will result in noise reduction over an increased frequency range, and often it is important that this frequency range extend down to lower frequencies to account for decreases in the BPF. Conventional perforate facesheets are nonlinear devices, i.e., their acoustic characteristics are a function of the acoustic particle velocity and, hence, the SPL of the sound that impinges on their surface [see Eq. (30)]. It is therefore important for the liner designer to either (1) control the nonlinearity to achieve an optimum impedance spectrum (this requires detailed understanding of the physics of sound transmission through a perforated sheet), or (2) reduce the nonlinearity such that the resultant impedance spectrum is more easily controlled.

Initial versions of liner concepts are often designed such that they are only suitable for use in a lab. However, the aircraft liner designer must always keep in mind the need for maturing the concept such that it becomes flightworthy. As such, it remains critical to keep features such as manufacturability, durability, predictability, and cost in mind when one is developing a new liner concept. Nevertheless, it is useful to extend beyond these parameters, with the belief that sufficient acoustic benefit will encourage manufacturers to overcome these challenges.

There is a push to reduce the core depth, as this reduces the diameter of the nacelle and thereby reduces the weight and corresponding fuel requirements. This often comes at the expense of increased liner geometry complexity. Again, the use of additive manufacturing provides one way to incorporate this complexity into the design. Many have also explored metamaterial concepts[34] as they apply to the liner design process. For the purposes of this study, a metamaterial is considered to be a structure, most often heterogenous but assumed to be homogeneous by wavelength, complex (periodic or not), exhibiting in some frequency domains atypical propagation properties compared to that observed in a conventional liner. For example, small heterogeneities (masses) may be periodically arranged in a homogeneous medium (e.g., foam). In this case, the spring behavior of the medium, coupled with the masses, can generate resonances and other interesting features. The ONERA metamaterials shown in the current paper include assemblies of elementary resonators that can be periodically duplicated to generate a homogenized material with a desired impedance over a broad frequency range. Using metamaterial concepts, the liner can also be designed such that the impinging acoustic waves are redirected in a preferred direction. Yet another field of interest is the use of multifunctional materials. When fabricated with materials that can withstand high temperatures, acoustic liners placed in the inner walls of the aft bypass duct provide thermal insulation from the hot core while also providing acoustic absorption.

Another concern for the liner designer is the drag caused by the rough surface and air jetting through the surface of the perforated facesheet. Aircraft manufacturers are interested in liner configurations that minimize the additional drag caused by liners mounted in the walls of the nacelle. The need for a reduction

in liner drag becomes even more important as the idea of placing acoustic treatment on surfaces other than the walls of the nacelle becomes more prevalent.[13–15]

NASA and ONERA have conducted extensive studies of liner drag over the last decade. Some of these studies focused on developing measurement approaches to determine the effects of an acoustic pressure field on the drag due to the acoustic liner.[22, 35–37] Others sought to find ways to reduce the drag, whether by reducing the porosity or by altering the shape of the facesheet perforations.

In summary, the goal of future acoustic liners is to achieve increased acoustic performance relative to conventional liners while satisfying all of the airworthiness constraints, and to do so with a decrease (or at worst, no change) in liner drag.

IV. Analytical Approach

Most of the models presented in this paper are based on a transmission matrix approach. A semiphenomenological porous media model based on the JCAPL (Johnson-Champoux-Allard-Pride-Lafarge) formulation is also presented. Finally, a lumped element approach is presented for prediction of the impedance of a conventional SDOF chamber.

A. Transmission Matrix Approach

Transmission matrix models offer the convenience of modularity, wherein the acoustic pressure and velocity transfer across each distinct portion of the liner is represented by a separate matrix. Each of these models is based on the notion of equivalent fluid within the facesheet perforations, the tubes used in the LEONAR concept, or the core chambers. The acoustic behavior of this equivalent fluid can be represented by two key parameters. For example, some models use the propagation constant and characteristic impedance, while others use the equivalent fluid density and bulk modulus.

The ZKTL (Zwikker and Kosten Transmission Line) model[25, 38] employs Zwikker and Kosten's formulation for propagation of sound in channels to predict the surface impedance of a liner. The propagation constant and characteristic impedance are used to represent the equivalent fluid in this model. This model is particularly useful for liners that include multilayer chambers, such as the 2DOF liners noted earlier. The following description presents a two-layer version of the model with the aid of Fig. 6. This figure provides a sketch of a single chamber of an SDOF liner, with a core height of h and a facesheet thickness of t. The thickness of the perforated facesheet is exaggerated to demonstrate distinct features of the model used in this study. This model treats each unique portion (air gap and perforated sheet) of the liner chamber in a sequential approach.

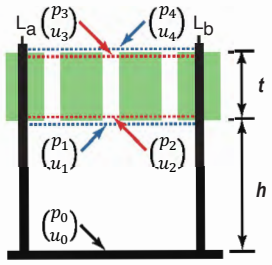

Figure 6: Sketch of single chamber with key parameters for transmision line impedance prediction model.

For the purposes of this study, the transmission line computation is initiated by assuming the backplate to be rigid and impervious. The acoustic pressure and particle velocity are therefore given as

$$\begin{pmatrix} p_0 \\ u_0 \end{pmatrix} = \begin{pmatrix} 1 \\ 0 \end{pmatrix}, \tag{2}$$

which yields an infinite impedance (zero admittance) at this location. All acoustic pressures and particle velocities in this analysis are normalized by $\rho_0 c_0^2$ and c_0, respectively, where the density of the air and the speed of sound are for the prevailing static pressure and air temperature. Changes in the acoustic pressure and particle velocity across the air gap with height h are computed via

$$\begin{pmatrix} p_1 \\ u_1 \end{pmatrix} = \begin{pmatrix} T_{11} & T_{12} \\ T_{21} & T_{22} \end{pmatrix} \begin{pmatrix} p_0 \\ u_0 \end{pmatrix}, \tag{3}$$

where the transmission coefficients (T_{11}, T_{12}, T_{21} and T_{22}) for an open layer (air gap) are given by

$$T_{11} = T_{22} = \cosh(k\Gamma h);\ T_{12} = \zeta_c \sinh(k\Gamma h);\ T_{21} = \zeta_c^{-1} \sinh(k\Gamma h). \tag{4}$$

Tijdeman[39] summarized the results of investigations conducted in the latter part of the 19th century regarding propagation of sound in gases confined in cylindrical tubes. He showed that the propagation constant could be expressed using four dimensionless parameters. These parameters are the reduced frequency,

$\bar{k}$, shear wave number, s, Prandtl number, Pr, and specific heat ratio, γ_0, defined as

$$\bar{k} = \frac{\omega d_c}{2c_0},\ s = \frac{d_c}{2}\sqrt{\frac{\rho_s \omega}{\mu}},\ \mathrm{Pr} = \frac{\mu C_p}{\kappa_0'},\ \gamma_0 = \frac{C_p}{C_v}. \tag{5}$$

Tijdeman also noted that an analytical solution to the simplified basic equations had been provided by Zwikker and Kosten[40] for the low-reduced-frequency case; i.e., when $\bar{k} \ll 1$ and $\bar{k}/s \ll 1$, which covered the ranges of reduced frequency and shear wave number previously published in the literature (prior to 1949). Tijdeman expressed the Kirchhoff equation in terms of these four parameters and solved this equation numerically for unrestricted ranges of reduced frequency and shear wave number, using the Zwikker and Kosten low reduced-frequency solution as an initial estimate. He found that the low-reduced-frequency solution appeared adequate for the range of reduced frequency and shear wave number of interest in conventional liners. The resultant solutions for the propagation constant, Γ, and characteristic impedance, ζ_c, are given by

$$\Gamma = \sqrt{\frac{J_0(\mathrm{i}^{3/2}s)}{J_2(\mathrm{i}^{3/2}s)}}\sqrt{\frac{\gamma_0}{n_\Gamma}}, \qquad \zeta_c = \frac{-\mathrm{i}}{\Gamma}\frac{J_0(\mathrm{i}^{3/2}s)}{J_2(\mathrm{i}^{3/2}s)}, \tag{6}$$

where

$$n_\Gamma = \left[1 + \frac{\gamma_0 - 1}{\gamma_0}\frac{J_0(\mathrm{i}^{3/2}\mathrm{Pr}^{1/2}s)}{J_0(\mathrm{i}^{3/2}\mathrm{Pr}^{1/2}s)}\right]^{-1}, \tag{7}$$

and impedances are normalized by the characteristic impedance of air, $\rho_0 c_0$.

The acoustic pressure and acoustic mass flow are assumed to be constant across the $\{1, 2\}$ interface in Figure 6, such that

$$p_2 = p_1, \qquad N_p S_p u_2 = S_{ch} u_1, \tag{8}$$

where N_p is the number of perforates (3 in this example) connected to a single air cavity, S_{ch} is the cross-sectional area of the chamber and S_p is the cross-sectional area within a single perforate.

Next, the wave propagation within the single orifice is computed using Eqs. (3) and (4), where the orifice diameter is used as the "chamber diameter" in the calculation of the shear wave number, i.e.,

$$\begin{pmatrix} p_3 \\ u_3 \end{pmatrix} = \begin{pmatrix} T_{11} & T_{12} \\ T_{21} & T_{22} \end{pmatrix} \begin{pmatrix} p_2 \\ u_2 \end{pmatrix}. \tag{9}$$

Again, the acoustic pressure and acoustic mass flow are assumed to be constant across the $\{3, 4\}$ interface, such that

$$p_4 = p_3, \qquad S_{ch} u_4 = N_p S_p u_3. \tag{10}$$

(Additional layers can be included in a similar manner until the acoustic pressure and acoustic velocity at the chamber surface are known.) The normalized surface admittance for the individual chamber (the portion between points L_a and L_b in Fig. 6) is computed as

$$\beta_{ch} = \frac{u_4}{p_4}. \tag{11}$$

Assuming the liner is comprised of multiple chambers, the effective admittance, β_s, across the liner surface is given by

$$\beta_s = \sum_{i=1}^{N_{ch}} \Omega_i \beta_{ch,i}, \tag{12}$$

where N_{ch} represents the number of chambers that combine to form the liner and Ω_i and $\beta_{ch,i}$ are the surface open area ratio and surface admittance of the i^{th} chamber, respectively. The uniform, effective, surface impedance of the liner is then given by $\zeta_s = 1/\beta_s$. Previous research[41] demonstrated that this computation of an effective impedance is appropriate when the distinct chambers (chambers that provide a unique impedance) are confined withing a spatial extent that is no larger than one-third of a wavelength for the highest frequency of interest.

Finally, the reflection and absorption coefficients, respectively R and α, relative to a normal incidence excitation are expressed by

$$R = \frac{\zeta_s - \rho_0 c_0}{\zeta_s + \rho_0 c_0}, \ \alpha = 1 - |R|^2 . \tag{13}$$

It should be understood that the Transmission Line Model is suitable for more complex configurations than what is shown in Figure 6. For example, this modeling approach is used to investigate each of the LEONAR designs depicted in Figure 7. The transmission coefficients for each component (tube or cavity)

are computed as described above, and the resultant elementary matrices are simply multiplied together to compute the surface impedance of the liner.

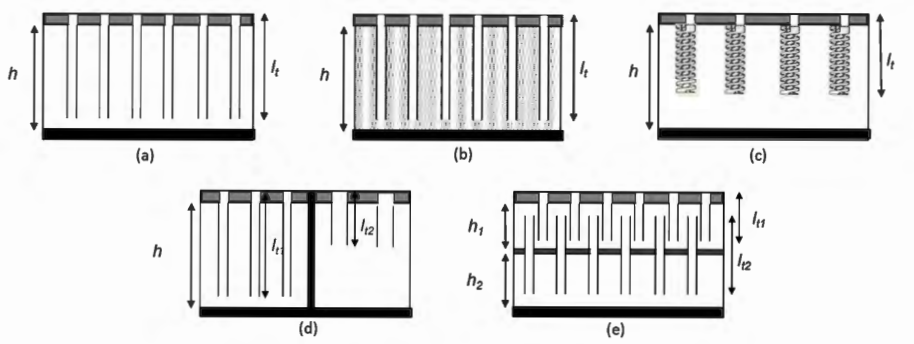

Figure 7: Different LEONAR designs - SDOF resonator with straight tubes and (a) air cavity or (b) porous material, (c) SDOF with spiral tubes, (d) parallel 2DOF resonators, (e) stacked 2DOF resonators.

B. Semiphenomenological Porous Media Model

In the simplified case where a porous material is assumed rigid, only airborne waves propagate in the material. The contribution of the solid phase to the acoustics is negligible and one can see the porous medium as an equivalent fluid subject to visco-inertial and thermal losses due to the high surface contact ratio between the fluid and solid phases and to the complex shape of the pores. Following Zwikker and Kosten[40] and assuming total decoupling between visco-inertial and thermal effects, one obtains the complex-valued Helmholtz equation of linear acoustics controlling the time harmonic wave propagation inside the equivalent-fluid material,

$$\Delta p + \omega^2 \frac{\widetilde{\rho}_{eq}}{\widetilde{K}_{eq}} p = 0, \tag{14}$$

where $\widetilde{\rho}_{eq}$ is the equivalent complex density of the fluid, encompassing all viscous effects between the two phases, and $\widetilde{K}_{eq}$ is the equivalent complex bulk modulus of the fluid, encompassing all thermal effects inside the pores.

Semiphenomenological models for $\widetilde{\rho}_{eq}$ and $\widetilde{K}_{eq}$ are obtained for different simplified pore geometries by using the limits of low or high frequency regimes, where the fluid is fully viscous-isothermal or potential-adiabatic, respectively. In keeping with the developments leading to Eqs. (3-4), one can show that for rigid isotropic porous media, the transfer matrix can be written[42] as

$$T_{es}(\omega) = \begin{bmatrix} \cos\left(\tilde{k}_{eq}t\right) & \mathrm{i}\tilde{\zeta}_{eq}\sin\left(\tilde{k}_{eq}t\right) \\ \mathrm{i}\sin\left(\tilde{k}_{eq}t\right)/\tilde{\zeta}_{eq} & \cos\left(\tilde{k}_{eq}t\right) \end{bmatrix}, \tag{15}$$

where $\tilde{\zeta}_{eq}$ $\tilde{c}_{eq}$ and $\tilde{k}_{eq}$ are the equivalent impedance, speed of sound and wavenumber, respectively. Once $\widetilde{\rho}_{eq}$ and $\widetilde{K}_{eq}$ are known, one can use Eq. (15) directly, since $\tilde{c}_{eq} = \sqrt{\widetilde{K}_{eq}/\widetilde{\rho}_{eq}}$, $\widetilde{K}_{eq} = \omega/\tilde{c}_{eq}$ and $\tilde{\zeta}_{eq} = \widetilde{\rho}_{eq}\tilde{c}_{eq}$.[42]

The JCAPL (Johnson-Champoux-Allard-Pride-Lafarge) model[43–46] takes into account cross-section variations and possible moderate constrictions between the pores and defines the equivalent fluid density and bulk modulus as

$$\widetilde{\rho}_{eq}(\omega) = \frac{\rho_0\alpha_\infty}{\phi}\left[1 - \mathrm{i}\frac{\omega_c}{\omega}\left(1 - b + b\sqrt{1 + \mathrm{i}\frac{\omega_c}{\omega}\frac{N}{2b^2}}\right)\right], \tag{16}$$

and

$$\widetilde{K}_{eq}(\omega) = \frac{K_0/\phi}{\gamma_0 - (\gamma_0 - 1)\left[1 - \mathrm{i}\left(\frac{\omega_c^{'}}{\omega}\right)\left\{1 - b^{'} + b^{'}\sqrt{1 + \mathrm{i}\frac{\omega}{\omega_c^{'}}\frac{N^{'}}{2\left(b^{'}\right)^2}}\right\}\right]^{-1}}, \tag{17}$$

$$\omega_c = \frac{\nu_0\phi}{\kappa_0\alpha_\infty},\ \omega_c^{'} = \frac{\nu_0\phi}{\kappa_0^{'}},\ N = \frac{8\kappa_0\alpha_\infty}{\phi\Lambda^2},\ N^{'} = \frac{8\kappa_0^{'}}{\phi\left(\Lambda^{'}\right)^2}, \tag{18}$$

$$b = \frac{N^{'}}{4\left(\frac{\alpha_0}{\alpha_\infty} - 1\right)},\ b^{'} = \frac{N^{'}}{4\left(\alpha_0^{'} - 1\right)},\ \kappa_0 = \mu/\sigma_0,\ K_0 = \gamma_0 P_0. \tag{19}$$

The case of a perforated plate or screen

The equivalent fluid model has been extended to perforated plates and screens by Atalla et al.[47] The classical geometrical parameters of such materials (size and shape of the perforations, thickness) were taken into account, as well as the type of interfacing media on each side of the plate/screen. Indeed, correction lengths due to acoustic radiation and viscous reactance in the vicinity of the perforations depend on the type of medium in contact. These interfacing effects were included in an equivalent tortuosity of the perforated plate. The parameters of the JCAPL are not all needed here, due to the geometrical simplicity of perforated plates and screens compared to more complex porous media. As such, the JCA model[43, 44] is sufficient. This is equivalent to setting $M = M^{'} = b = b^{'} = 1$ in Eqs. (16) and (17). As for the other parameters, they are given as $\Lambda = \Lambda^{'} = r$, with r the perforation radius; $\sigma_0 = 8\mu/\phi r^2$, with ϕ the porosity simply equal to the perforation ratio Ω.

As stated previously, all interfacing and end-correction effects are included in the tortuosity α_∞, which

becomes

$$\alpha_\infty(\omega) = 1 + \frac{\epsilon_e}{t}\left(\Re\left(\widetilde{\alpha}_{p,1}\right) + \Re\left(\widetilde{\alpha}_{p,2}\right)\right), \tag{20}$$

$$\epsilon_e = 0.48\sqrt{\pi r^2}\left(1 - 1.14\sqrt{\phi}\right),\ \widetilde{\alpha}_p = \widetilde{\rho}_{eq}/\rho_0. \tag{21}$$

ϵ_e is a (static) correction associated with interactions between perforations and $\widetilde{\alpha}_{p,i}$ is the dynamic tortuosity of a material in contact with the i^{th} side of the perforations. In the case of air, $\widetilde{\alpha}_{p,i} = 1$.

C. Motsinger Kraft Model

The Motsinger Kraft Model (MKM)[48, 49] is based on a two-parameter flow resistance model that leads to an estimate for the facesheet acoustic resistance of an SDOF liner. This lumped element model can be used to predict the surface impedance of SDOF liners (or individual chambers) with or without grazing flow. The normalized acoustic impedance of a perforate-over-honeycomb liner is given by

$$\zeta_s = \theta + \mathrm{i}\chi = \theta_{\text{fs}} + \theta_{\text{gf}} + \mathrm{i}\left\{\chi_{\text{fs}} - \cot\left(kh\right)\right\}, \tag{22}$$

where the mass reactance of the facesheet, χ_{fs}, is given by

$$\chi_{\text{fs}} = \frac{k(t + \epsilon d)}{\Omega}, \tag{23}$$

and

$$\epsilon = \frac{0.85\left(1 - 0.7\sqrt{\Omega}\right)}{1 + 305\, M_{C/L}^3}. \tag{24}$$

There are viscous and nonlinear contributions to the facesheet resistance, as well as a grazing flow contribution. If the perforate facesheet is treated as a lumped element, the acoustic oscillatory flow through the perforate can be treated as locally incompressible and quasisteady. If so, the acoustic resistance can be estimated via a measurement of the DC flow resistance, $R_f = A + B \cdot V_{\text{inc}}$, where A and B are determined from the measurement and V_{inc} represents the incident flow velocity through the facesheet. If pipe flow and orifice metering theory concepts are considered, this two-parameter flow resistance model leads to an

estimate for the facesheet acoustic resistance as

$$\theta_{\rm fs} = \frac{R_f}{\rho_0 c_0} = \frac{a\mu t}{2\rho_0 c_0 \left(\Omega C_D\right) d^2} + \frac{\kappa_i + \kappa_e}{2c_0 \left(\Omega C_D\right)} u_{\rm rms}, \tag{25}$$

where

$$u_{\rm rms} = \frac{P_{\rm ref} 10^{\rm SPL/20}}{\rho_0 c_0 \ |\zeta_s|} \tag{26}$$

and the total SPL (sum of incident and reflected waves) at the surface of the liner is used in the computation. Note that $u_{\rm rms}$ is a function of the liner impedance, which in turn depends on the facesheet resistance, $\theta_{\rm fs}$ (Eq. (25), a component of the impedance (Eq. (22). An iterative approach is typically used to find the impedance and rms acoustic particle velocity.

Motsinger and Kraft[48] assumed

$$C_D = 0.76,\ a = 64,\ \kappa_i + \kappa_e = 1. \tag{27}$$

The grazing flow contribution to the resistance is given by the Rice-Heidelberg model[50, 51] as

$$\theta_{\rm gf} = \frac{M_{\rm C/L}}{\Omega \left\{2 + 1.256 \left(\delta_1/d\right)\right\}}. \tag{28}$$

However, if $\delta_1/d \approx 1$ and the grazing flow effect is dominant, $\theta_{\rm gf}$ can be estimated as

$$\theta_{\rm gf} = \frac{M_{\rm C/L}}{3\Omega}. \tag{29}$$

The end correction, ϵd, in the facesheet mass reactance has a value of 0.85 for the no-flow, linear correction for a single, isolated, orifice. The $\left(1 - 0.7\sqrt{\Omega}\right)$ factor is provided by Ingard,[1] and the grazing flow effect $\left(1 + 305 M_{\rm C/L}^3\right)$ is due to Rice.[50]

In summary, the acoustic impedance of the liner is given by

$$\zeta = \frac{32\mu t}{\rho_0 c_0 \left(\Omega C_D\right) d^2} + \frac{1}{2c \left(\Omega C_D\right)^2} u_{\rm rms} + \frac{M_{\rm C/L}}{\Omega \left\{2 + 1.256 \left(\delta_1/d\right)\right\}} + {\rm i} \left\{ \frac{k(t + \epsilon d)}{\Omega} - \cot\left(kh\right) \right\}. \tag{30}$$

V. Experimental Approach

The majority of the liner concepts discussed in the current article have been investigated using the NASA and ONERA normal incidence impedance tubes. These test rigs support investigation of the effects of sound pressure level (SPL) and frequency on the acoustic impedance (and resultant absorptive properties) of acoustic liners. Some of the key parameters for these test rigs are provided below.

A. Normal Incidence Tube - NASA

The NASA Langley Normal Incidence Tube (NIT, see Fig. 8) uses six 120-W compression acoustic drivers to produce a sound field that impinges on the surface of the acoustic liner. The 50.8 mm×50.8 mm waveguide is approximately 914 mm long, and contains three flush-mounted microphones. A reference microphone located 6.35 mm from the surface of the liner is used to ensure that the liner is exposed to the desired sound pressure level (SPL). Two measurement microphones are positioned 63.50 mm and 95.25 mm from the liner surface, and are mounted within a rotating plug (see Fig. 8(b)) such that their positions can be precisely interchanged.

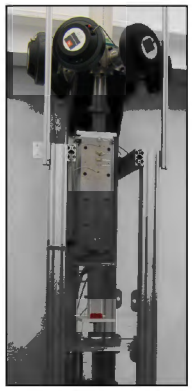

(a) Photograph of NIT.

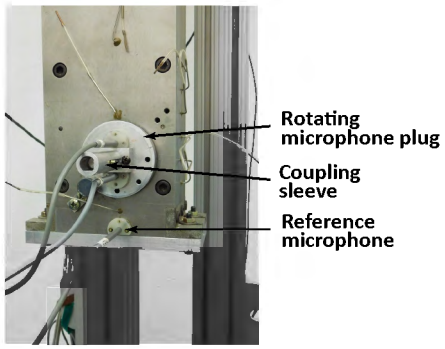

(b) Close-up view of measurement section.

Figure 8: NASA Normal Incidence Tube (NIT).

The NIT supports three source types; stepped sine, swept sine, and broadband. For the stepped-sine source, measurements are conducted one frequency at a time. The input voltage to a function generator is set to achieve the desired total SPL (within ±0.5 dB of target) for this target frequency at the reference microphone. The current system supports testing with total SPLs up to approximately 155 dB, and at frequencies of 0.4 to 3.0 kHz (typically in 0.2 kHz increments).

The controlled-amplitude, swept-sine source[52] allows the source amplitude to be maintained to the same accuracy (within ±0.5 dB of target) and the frequency is swept through the range of interest. This method provides data at approximately 5 Hz increments over the same frequency range and requires much less time than the stepped-sine approach. However, the maximum SPL that can be currently achieved is approximately 145 dB.

The broadband source is based on a white noise electronic signal fed to the six acoustic drivers. For this approach, the full frequency spectra of acoustic pressures at each microphone are read simultaneously. The current implementation records readings at 12.5 Hz increments over the same frequency range. The overall SPL measured over the frequency range of 0.4 to 3.0 kHz is set at the reference microphone location.

The Two-Microphone Method[53, 54] is used with these measured acoustic pressures to determine the acoustic impedance at the surface of the liner. These results are used to evaluate the efficacy of the impedance prediction models described in Section IV.

B. Normal Incidence Tube - ONERA

ONERA performs normal incidence impedance measurements using three cylindrical tubes with different internal diameters (37, 43 and 98 mm, see Fig. 9). This allows the sound field to be confined to plane waves for frequency ranges of 200 to 2,000 Hz for the largest tube and 200 to 5,000 Hz for the smallest tube. Samples may be mounted with a piston to allow control of the sample depth, or may be built as integrated designs to avoid acoustic leaks.

The smallest tube diameter is preferred for homogeneous or multilayered materials (e.g., SDOF or piled 2DOF liners), while the largest diameter is used to test larger samples such as the labyrinth metasurface. The smallest tube can also be equipped with a heated sample holder and a cooling system located all around the tube, such that the acoustic impedance of a material subjected to a thermal gradient can be measured.[16] The standard measurement method for two microphones is used.[55,56] By judicious selection of the appropriate two (of three available) microphones, the total frequency range for which only plane waves propagate in the ONERA normal incidence tubes can be taken into account. The source is generally broadband type for which the total SPL is controlled at one microphone location, for a given frequency range up to the maximum frequency defined above.

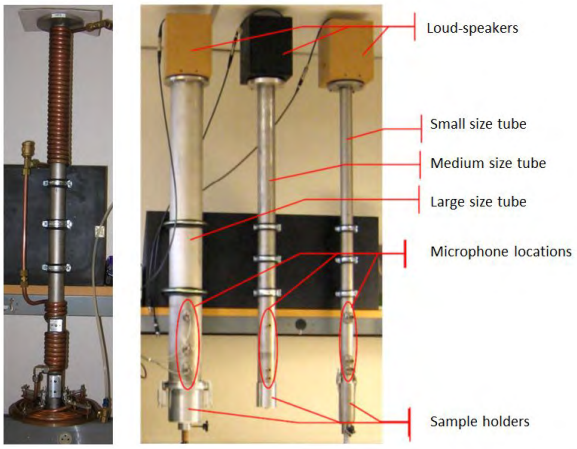

Figure 9: ONERA Normal Incidence Tubes.

VI. Novel Liner Concepts

This section focuses on three NASA concepts that employ distributed impedance and three ONERA concepts that employ different versions of the long elastic open neck acoustic resonator (LEONAR). Each of these concepts has been previously described in the literature. Therefore, the descriptions presented herein are mainly intended to convey (1) the physical mechanisms upon which they are based, (2) the key features that separate them from other concepts, and (3) their current testing status. Many of these concepts have also been evaluated in the presence of grazing flow, and some of the key effects of flow are presented. However, the majority of the results are confined to no-flow results based on the impedance prediction models (Sec. IV) and normal incidence tube tests (Sec. V), and the results are intended to demonstrate how the aeroacoustic metrics (Sec. VII) can be used to compare liner concepts prior to attaining this more expensive information. Unless otherwise noted, all results shown in this paper are compared on the basis of total SPL - sum of incident plus reflected waves.

A. NASA

Each of the NASA concepts included herein is based on the idea of varying the impedance over the surface of the liner to achieve a desired effective uniform impedance. As noted earlier, when the impedance of individual chambers of a liner are allowed to vary in a controlled manner, the full liner presents an effective impedance that results in sound absorption over an increased frequency bandwidth. This increased frequency range of sound absorption is the key goal for these three concepts (this was also true for the MDOF mesh-cap concept). The first two concepts vary the reactance between adjacent chambers and the third concept varies the resistance between adjacent chambers.

1. Variable depth liners (straight and bent chambers)

Variable-depth liners[25] (see Fig. 10) are becoming increasingly viable for aircraft applications due to recent advances in additive manufacturing (3D printing). As its name implies, the individual core chambers of this liner have different depths, such that each chamber may be tuned (quarter-wavelength resonator) to a different frequency. By judicious selection of the different chamber depths, the liner can be designed to absorb sound over a wide frequency range. For example, if there are only two distinct chamber depths that are replicated to form the entire liner, then the liner will be tuned to provide peak attenuation near (addition of a facesheet causes these frequencies to slightly decrease) the two frequencies for which the quarter-wavelengths match the two chamber depths. If those frequencies are sufficiently close together, it is also possible to attain increased sound absorption at the intervening frequencies. Inclusion of additional chamber depths allows for the resultant absorption spectrum to be easily tuned.

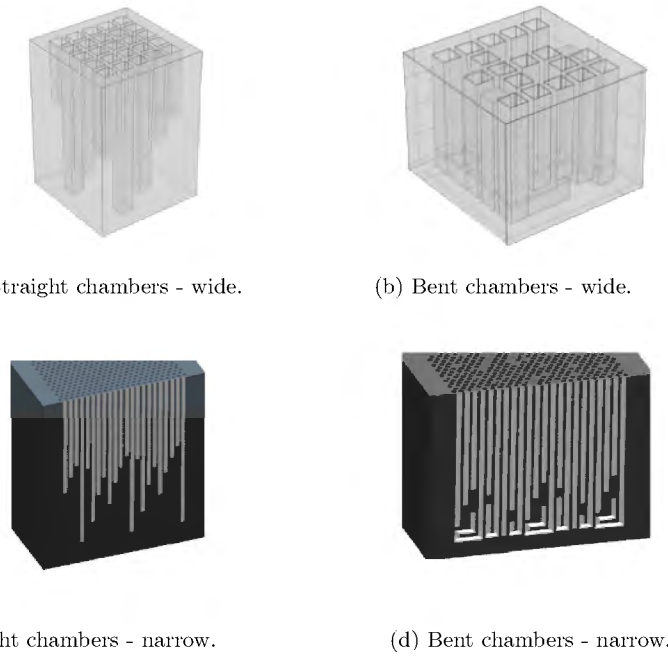

(a) Straight chambers - wide.

(b) Bent chambers - wide.

(c) Straight chambers - narrow.

(d) Bent chambers - narrow.

Figure 10: Variable-depth straight- and bent-chamber liner configurations.

The first version (Fig. 10(a)) employs wide chambers, similar to those of a conventional SDOF liner, and is typically covered with a perforated facesheet (not shown in figure). Although the frequency tuning is dominated by the choice of chamber depths, the majority of the acoustic resistance is achieved via the perforated facesheet. For the second version of the concept (Fig. 10(c)), the chambers are reduced in diameter.

This allows significant viscous losses along the walls of the chamber, thereby eliminating the requirement of a perforated facesheet. Each of these configurations also allows for the chambers to be bent (Fig. 10(b,d)) such that longer chambers can be fit into a reduced volume. This allows the frequency range of absorption to be extended to lower frequencies than would be possible with simple SDOF and 2DOF configurations.

The MKM (Sec. IV.C) is often used to compute impedances for variable-depth liners with straight chambers. This model was originally developed for uniform-depth liners, and therefore, does not account for phasing differences that will occur between adjacent chambers due to the different path lengths (distance from the facesheet to the rigid backplate). Nevertheless, if this model is applied to each individual chamber, the results for the individual chambers can then be combined [see Eq. (12)] to determine the surface impedance distributed across the group of chambers. The Transmission Line Model (ZKTL, see Sec. IV7) can also be used to compute impedances for variable-depth liners with either straight or bent chambers. For this model, each chamber is evaluated independently, and the results are combined to get an effective distributed impedance. One limitation of this approach, however, is the fact that the ZKTL model (as described herein) does not account for grazing flow effects. In cases where there is grazing flow, the ZKTL is used to compute the core impedance and the MKM is then used to compute the impedance change across the facesheet.

The length of a bent chamber can be predicted (via ZKTL) as the sum of the individual segments that make up the chamber. However, this neglects the effects of nonuniform acoustic pressure and changing propagation wavenumbers through the bends. Cummings[57] offers an approach to account for these effects in the impedance computation based on the radius of curvature and angle of the bend. Interestingly, the choice of these two parameters can cause the effective chamber length to be either shorter or longer than the actual chamber length (as measured along the centerline), and properly accounting for these bends becomes more difficult as the number and angles of bends increases. For these complex configurations, higher-fidelity tools (e.g., COMSOL[58]) can be employed to more accurately predict the surface impedance. Regardless, the ZKTL and MKM models are sufficient for parameter studies.

One additional issue that must be considered when bent chambers are used is packaging. To use the available volume efficiently, it is often necessary to bend a single chamber in multiple directions (fully 3D configuration). A useful tool, Packing3D,[20] has been developed for this application. This code only allows for 90° or 180° bends in the individual chambers, but can very quickly combine chambers of variable lengths (depths) to fit into the available volume. For example, packaging of a 25-chamber configuration that includes five unique chamber depths can be achieved in a few seconds.

Figure 11 provides a comparison of predicted and measured results for straight and bent-chamber liners based on a configuration similar to that shown in Figure 10(a,b). The liners consist of a distributed array of chambers with lengths of 39, 71, and 123 mm, and do not include a facesheet. Total liner thicknesses are

127 mm and 66 mm, respectively, for the straight and bent-chamber liners. The measured results for the straight and bent-chamber samples are depicted with red dotted lines and green symbols, respectively, and the corresponding prediction is depicted with a solid blue line. The measured results are very similar for the straight and bent-chamber configurations, and the comparison with predicted results is also quite favorable. This indicates the choice of straight or bent chambers has limited effect on the acoustic performance.

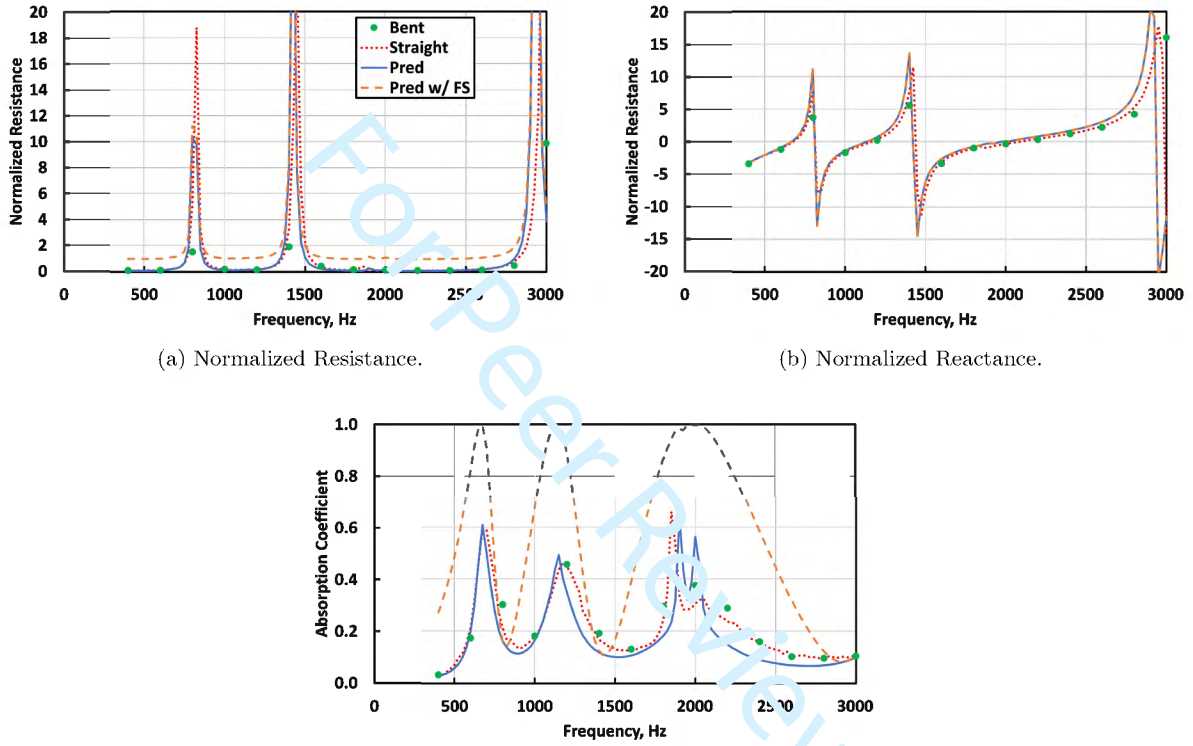

(a) Normalized Resistance.

(b) Normalized Reactance.

(c) Absorption Coefficient.

Figure 11: Comparison of predicted and measured results for straight and bent-chamber configurations. Measured bent- and straight-chamber results (with no facesheet) are represented with green circles and red dotted lines, respectively. Predicted results (assuming straight-chamber configuration) are represented with blue lines (no facesheet) and orange dashed lines (with facesheet), respectively.

The last curve on this figure, a dashed orange line, depicts the predicted effects of adding a facesheet with a normalized resistance of 0.9 over the surface of the liner. This causes the predicted absorption coefficient spectrum to have much higher and broader peaks. The valleys in the absorption spectrum could have higher absorption coefficient values by inclusion of additional chamber depths.

The main limitation of this concept is that the chamber length can become quite large for some of the lower frequencies of interest. This limitation can be overcome by the use of bent (folded) chambers, as has been considered by numerous researchers. However, the use of bent chambers introduces another concern.

As shown in Figure 10(b), the use of bent chambers sometimes causes the need for portions of the surface to be made solid, thereby causing the effective acoustic resistance of the liner to increase. Figure 10(d) provides another option - reduction of the chamber diameter. When sufficiently narrow chambers are used, it is generally possible to combine the chamber designs such that the surface porosity is maintained constant. However, smaller chambers also produce an increase in acoustic resistance. Thus, it falls to the liner designer to find an appropriate compromise between the ability to tune to the desired set of frequencies and the need to achieve a desired effective resistance spectrum.

Variable-depth liners constructed using wide chambers have been tested in the NASA Grazing Flow Impedance Tube (GFIT) in the presence of mean flow.[41, 59, 60] The wide chambers were covered with conventional perforated facesheets that provided a large portion of the acoustic resistance. As such, the nonlinearity of these facesheets caused a corresponding nonlinearity for the full liners. Thus, grazing flow effects are virtually the same for this type of liner as for a conventional SDOF liner, i.e., the acoustic resistance increases and the effective impedance becomes less sensitive to source level with increasing grazing flow. If narrow chambers, such as those shown in Figure 10(d), are used, the effects of flow should be expected to be much less. This is due to the large increase in the chamber thickness to diameter ratio.

2. Shared inlet port

The shared inlet port configuration[61] also employs variable depth chambers, as shown in Figure 12. As such, it presents similar benefits and drawbacks. Part (a) of the figure presents a conventional variable-depth configuration (similar to that shown in Figure 10(a) with the perforate facesheet included), whereas part (b) presents a shared inlet configuration that uses the same individual chamber lengths. Two features can be observed in the shared inlet port configuration. First, two distinct chambers feed into the facesheet via a single port that has similar cross-sectional geometry to that of a single chamber. In other words, the portion of the core that communicates with the impinging sound wave via the facesheet is roughly half the size of that for the conventional liner. Also, the concept can be carried further, such that more than two chambers feed through a single inlet port.

The second feature is a direct consequence of the first. Specifically, the porosity of the entire liner surface is decreased according to the reduction in the size of the inlet port. This offers two immediate benefits. The reduction in porosity causes the liner drag to be reduced. The need for roughly half the number of facesheet holes (or even fewer if more chambers are combined via a single inlet port) also provides a manufacturing cost reduction.

(a) Conventional variable-depth configuration.

(b) Shared inlet port configuration.

Figure 12: Conventional and shared inlet port liner configurations.

Figure 13 provides a comparison of absorption coefficient spectra measured with approximately 85 mm-thick variable depth and shared inlet port liners similar to those shown in Figure 12. Each liner consists of eight distinct chamber depths. Each of these chamber depths produces increased absorption at or near their respective quarter-wavelengths (there are eight peaks in the absorption spectrum, but only seven occur within the displayed frequency range). There are distinct dips in the absorption when two adjacent tuning frequencies are sufficiently far apart, slightly more so than for the case of conventional variable-depth liners, where there is no internal communication between adjacent chambers. Nonetheless, the broadband absorption achieved with this approach is significant.

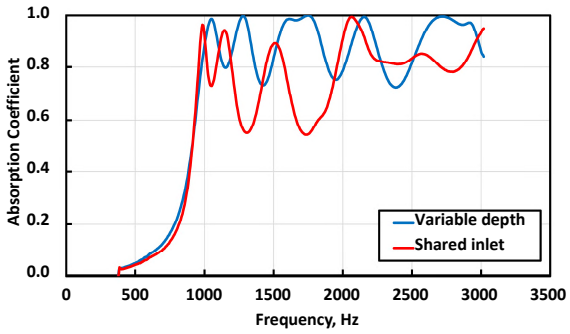

Figure 13: Comparison of measured absorption coefficient spectrum for variable depth and shared inlet port liners; 120 dB source.

Grazing flow tests have been conducted with shared inlet port liners mounted in the GFIT.[61] These tests demonstrated that significant attenuation could be achieved over a broad frequency range, similar to those achieved with conventional variable-depth liners, while also significantly reducing the mean relative

liner drag. More detailed studies of this concept are clearly warranted.

3. Variable facesheet

The current implementation of variable facesheet liners (see Figs. 14 and 15) is essentially the same as a conventional SDOF liner, with one exception. The geometric properties of the facesheet are allowed to vary from chamber to chamber. It has been well understood for decades that one could modify the impedance of an SDOF liner by changing the facesheet geometry. Specifically, the perforate hole diameter, open area ratio (aggregate surface of holes per honeycomb chamber surface), and facesheet thickness are key parameters in any traditional impedance prediction model.

Peak attenuation for a liner occurs at frequencies near resonance [e.g., near 1300 Hz in Figure 15(c)]. The main control mechanism to achieve resonance at a desired frequency is via control of the acoustic reactance. Variable facesheet liners allow the mass reactance of the facesheet to vary between adjacent chambers, while also allowing the acoustic resistance to be tuned to improve sound absorption. Since the mass reactance is generally much less than the full chamber reactance (including the effects of the empty chamber), this concept is expected to provide sound absorption over a smaller frequency range than can be achieved with the former two concepts. Nevertheless, the results of Figure 15(c) clearly demonstrate that a variable facesheet is capable of providing sound absorption over a wider frequency range that can be achieved via a uniform facesheet.

(a) Wide chamber core. (b) Variable facesheet.

Figure 14: Sketch of (a) core and (b) variable facesheet liner configurations.

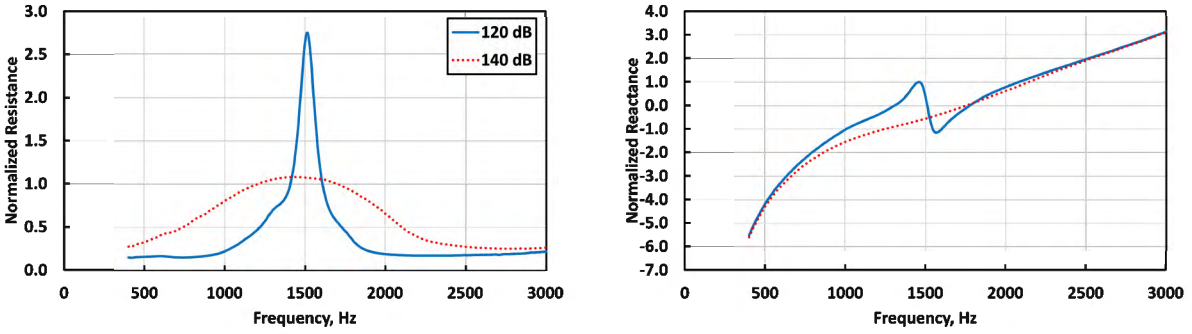

(a) Normalized Resistance.

(b) Normalized Reactance.

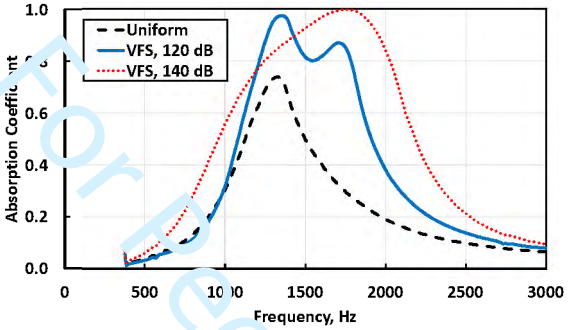

(c) Absorption Coefficient.

Figure 15: Comparison of measured results for a variable facesheet liner at two source levels with predicted absorption for a uniform facesheet (120 dB source) with two 1.27 mm-diameter holes per chamber.

Until recently, it was very difficult (and costly) to consider using facesheets for which these properties varied rapidly over the surface of the liner. However, recent advances in manufacturing processes have made this a much more viable concept. Indeed, additive manufacturing and robotic drilling processes allow for straightforward implementation of the variable facesheet concept. If the facesheet geometric properties (hole diameter, sheet thickness, open area ratio) are allowed to be different for adjacent chambers, the resultant distributed impedance can be tuned to achieve desired absorption spectra. An earlier study[62] has shown that proper distribution of the geometric properties over the surface of a liner can be used to achieve significant broadband noise reduction relative to what could be achieved with a uniform facesheet.

Measured impedance and absorption spectra for the 38.1 mm-thick, variable facesheet liner (Fig. 14) are presented in Figure 15. Data were acquired in the NASA NIT with a tonal source (one frequency at a time) at source SPLs of 120 and 140 dB. This liner is strongly affected by the source level. As the source level is increased, the resistance spectrum transitions from a narrowband peak near antiresonance (negative-slope zero crossing in corresponding reactance spectrum) to a broadband spectrum where the antiresonance totally disappears. Although the strong resistance peak at the lower source level inhibits the absorption

near antiresonance (around 1500 Hz), the liner provides significant broadband absorption for both source levels. This variable facesheet liner also provides a significant increase in broadband absorption relative to that which is typically achieved via a uniform facesheet, as shown in Figure 15(c). These results provide evidence of the value of this concept, but further optimizations of the configuration are needed.

Grazing flow tests have recently been conducted with variable facesheet liners.[63] As with conventional liners, the addition of mean flow causes the resistance to increase while having limited effect on the reactance. This causes liners that have been designed for the no-flow condition to have reduced effect in the presence of flow. Further investigations are needed in which the liner is designed to target the optimum impedance for a desired flow condition, to determine whether this concept is viable for usage in mean flow applications.

B. ONERA

Each of the ONERA concepts presented herein employs the LEONAR (long elastic open neck acoustic resonator) concept to provide broadband sound absorption centered on a lower frequency. Increasing the length of the tube that extends from the perforation in the facesheet causes an increase in the mass reactance, which results in a decrease in the resonance. Therefore, each of these concepts is particularly well designed for low frequency sound absorption. Some configurations also employ additional degrees of freedom (e.g., piled 2DOF LEONAR concept), and therefore also achieve increased broadband sound absorption.

This investigation focuses on the use of no-flow results to determine whether these concepts warrant consideration for full-scale applications, presumably with grazing flow. However, a number of tests have been conducted to explore the effects of grazing flow for liners based on the LEONAR concept.[18, 64] For example, Zhao et al.[65] found that grazing flow weakens the interaction between the resonator cavity and the main duct, which causes resonance to move to a higher frequency and the maximum transmission loss to be reduced. However, the acoustic resistance is linearized by the use of extended necks, such that the affect of grazing flow on the resonant frequency is reduced.[66, 67]

1. SDOF LEONAR with Variable Tube Shapes

Acoustic liners with conventional perforated plate facesheets generate large variations in absorption. Non-linearity (i.e., impedance is a function of the impinging acoustic particle velocity) in these liners is due to acoustic vortices around the perforations for a low ratio of plate thickness to hole diameter (t/d).

The SDOF LEONAR concept[64, 68] consists of linking the perforated facesheet with open hollow tubes introduced into the cavities (Fig. 16) to shift resonance to lower frequencies by a prolongation of air column lengths. This concept has a linear behavior practically independent of the incident acoustic pressure level, which is representative of a constant (independent of frequency) impedance and absorption coefficient.

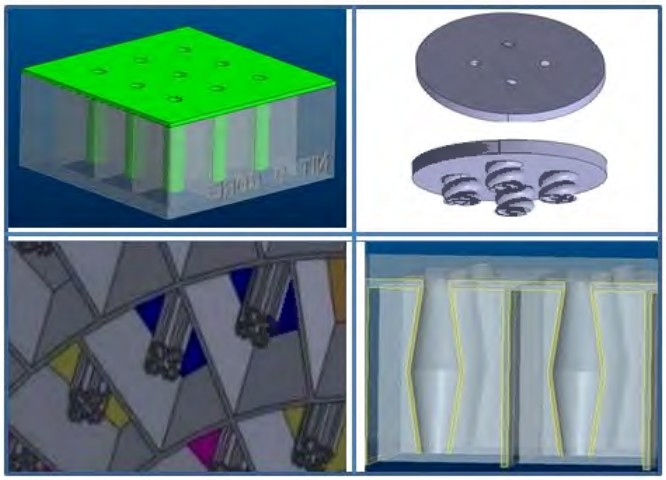

Figure 16: SDOF LEONAR liner configurations.

It is perhaps useful to review the effects of perforate facesheet thickness on the perceived nonlinearity of the liner. Figure 17 presents the predicted impedance and corresponding absorption coefficient spectra for two liners. Each liner consists of a perforated facesheet over a 20 mm-deep core and a rigid backplate. The first has a 'Thin' facesheet, with a porosity of 5%, a hole diameter of 1 mm, and a sheet thickness of 1 mm. The second, labeled 'Thick', is identical except for a sheet thickness of 20 mm. The conventional perforate liner ('Thin') is observed to be linear (no change in impedance spectrum) at source levels up to about 100 dB, and to gradually become more nonlinear as the source level is increased further. (Note: The calculations shown in this figure are for incident SPLs of 80 to 140 dB, not total SPLs.)[21] The thicker facesheet causes the intrinsic resistance to be much higher, and the liner is very linear up to a source level of 140 dB. Here, the SPL effect appears reduced on the absorption spectrum of the thicker plate because its resistance is already high in the linear domain. As such, an increase of the resistance caused by nonlinear SPL effects is relatively smaller than in the case of a low resistance liner. In practice, nonlinear effects are expected to be less detectable on the absorption spectra of LEONAR liners, even for equal levels of nonlinearity on the impedance. In addition, the t/d ratio (higher for LEONAR liner) might play a role in delaying the appearance of these nonlinear effects, as suggested in Ingard and Labate.[69]

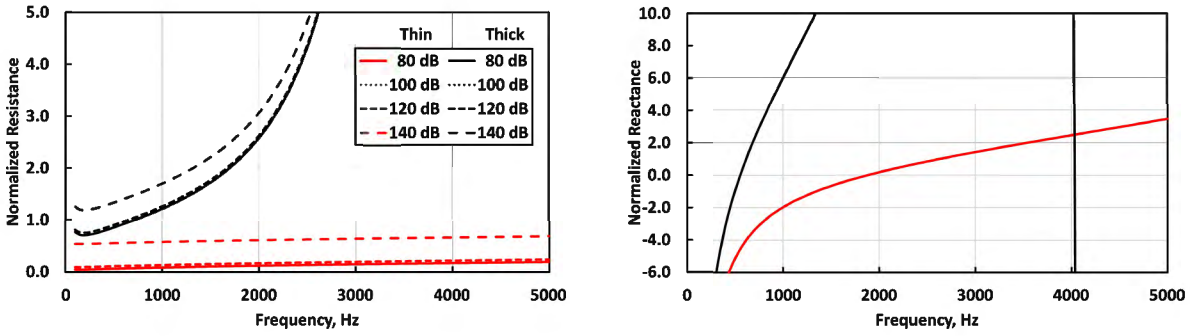

(a) Normalized Resistance.

(b) Normalized Reactance.

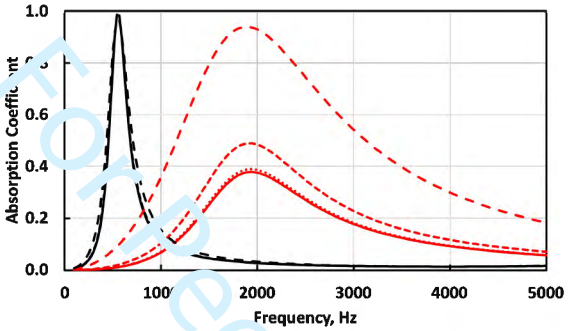

(c) Absorption Coefficient.

Figure 17: Use of Melling's model to compute the effects of facesheet thickness on liner nonlinearity.

Moreover, the tube lengths allow shifting of the frequency range of absorption. Conventional SDOF liners achieve resonance at a frequency for which the cavity depth is approximately $\lambda/4$, but the SDOF LEONAR can achieve the same resonant frequency with a depth less than $\lambda/20$. However, an increase in length can be associated with a reduction of the absorption coefficient, essentially because of a significant reduction of cavity volume (the tube fills up more of the cavity). The tube property, namely rigid or flexible, has no effect on the LEONAR acoustic characteristics in the low frequency range. Thus, it can be useful in some cases to use flexible material (as teflon or elastomer) to be more easily introduced in the cavity.

Variable tube shapes[70] allow for increased resistance (increased surface) relative to that achieved with a conventional circular shape for a given tube surface (and, therefore, for a given porosity and number of tubes), irrespective of the SPL of the impinging sound. This additional resistance is sufficient to modify the absorption coefficient without altering the resonant frequency. Conversely, when variable perforate shapes are used in conventional liners, this additional resistance occurs only for low incident SPLs. The behavior of tube shapes is governed by the "equivalent radius" or "perimeter/surface." Figure 18 provides simulated and experimental absorption coefficients for star hexagon and cross holes. Although theses holes have very different shapes, they provide similar surface and "equivalent radius" or "perimeter/surface." The absorption

coefficients are similar for a given cavity thickness, i.e. 30 mm.

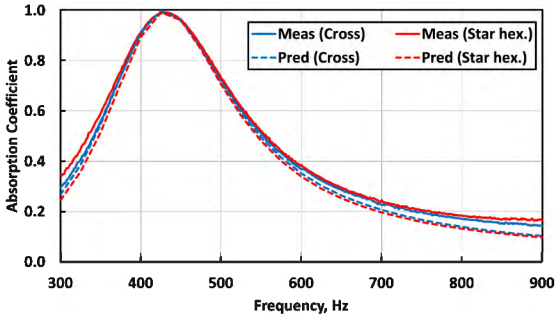

(a) Comparison of measured and predicted absorption coefficient spectra.

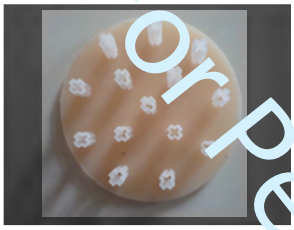

(b) Cross shaped tubes.

(c) Star hexagonal shaped tubes.

Figure 18: SDOF LEONAR liners with cross and star shaped tubes. Cavity thickness is 30 mm.

A variation of tube shape along its length can also be considered. For example, an increase of the internal (midpoint) radius of "double cone" tubes causes a decrease of resistance and a shift of the reactance curve toward higher frequencies. This reactance shift is predominately a translation of the curve to higher frequencies, with an accompanying increase of reactance with increasing frequency, sugggesting an increase in mass reactance [see Eq. (23)]. It is therefore possible to adjust the internal radius to mimic the response of a resonator with straight tubes, for a smaller external hole (see Fig. 19). This could be used to reduce the turbulence that could occur at the surface of a large perforation. Nevertheless, because of a wider internal hole, the impedance is more dependent on the incident SPL.

Figure 20 provides acoustic resistance spectra measured in the ONERA normal incidence tube for LEONAR designs that target different constant resistance values. While the tube shapes and lengths are different, the POAs, cavity thicknesses and zero reactance frequencies are similar (5%, 27 mm, 450 Hz). The change in resistance (nonlinearity) caused by the increase from 120 to 140 dB is practically constant at 0.15 for the longest tubes (samples 1, 2 and 4) and increases to 0.25 for the shortest tubes (sample 3). It would

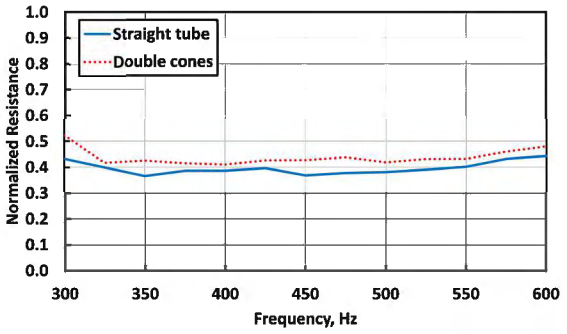

(a) Normalized Resistance.

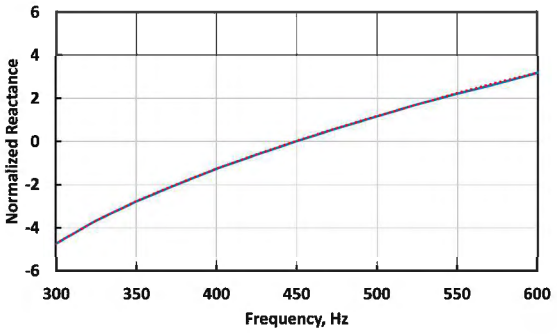

(b) Normalized Reactance.

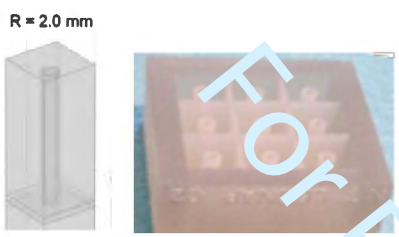

(c) Straight tubes; radius of 2.0 mm.

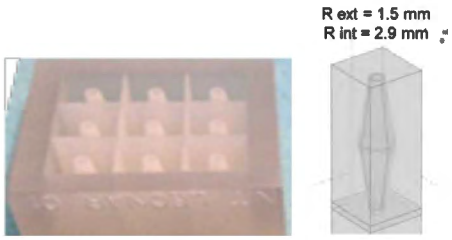

(d) Double-cone tubes; external and internal radii of 1.5 and 2.9 mm, respectively.

Figure 19: Comparison of straight tube and double-cone LEONAR liners.

appear that a short distance between the tube output and the rigid backplate tends to inhibit the vortex generation and shedding. Moreover, the additional normal resistance has a relatively low effect on the absorption coefficient for the highest resistances (samples 3 and 4).

Finally, using spiral tubes[71] instead of straight tubes increases the propagation length of the inner tubes for a limited height, allowing a reduction of total cavity thickness. Figure 21 compares measured absorption coefficients obtained in an impedance tube for straight and spiral tubes whose tube thicknesses and radii are equivalent. Based on the difference between the propagation lengths of the straight and spiral tubes, the resonant frequency of the straight tubes would be expected to decrease by 42% in the spiral tubes. However, the volume occupied by spiral tubes reduces the available air cavity, such that the measured decrease in resonant frequency is closer to 30%. As a result, it may be necessary to tune the tube geometry to achieve optimum acoustic performance for a particular application.

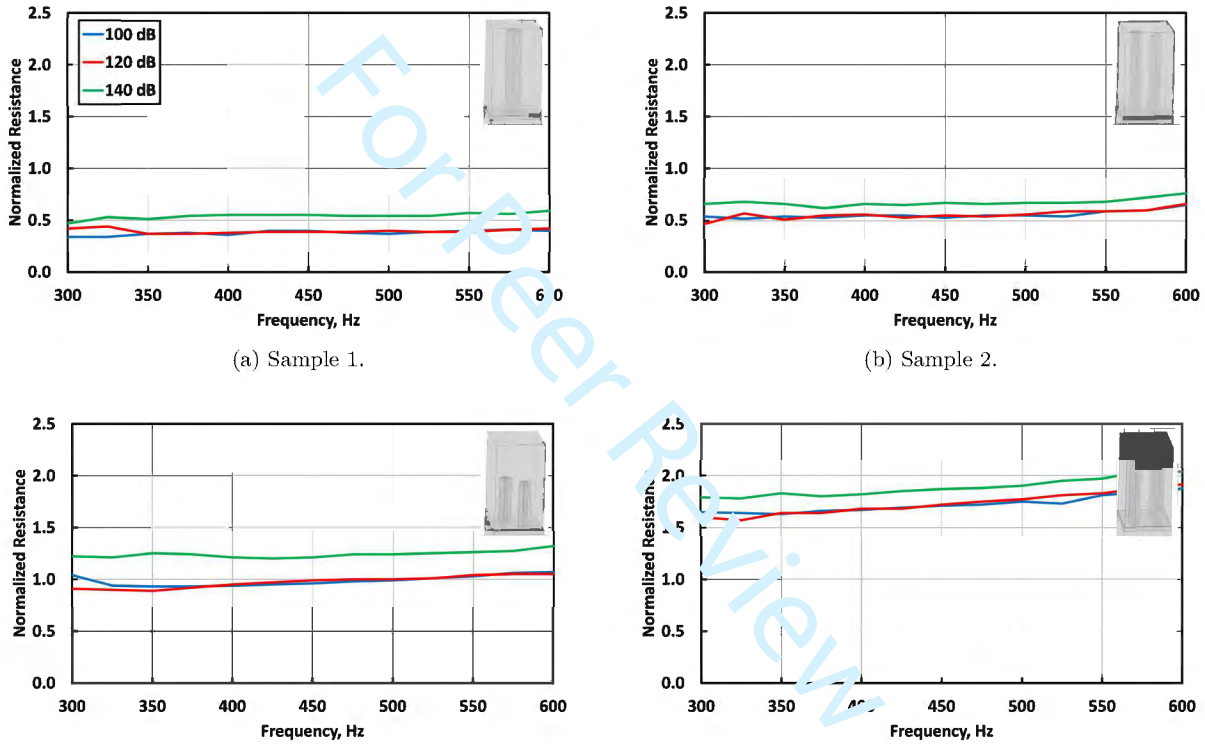

(a) Sample 1.

(b) Sample 2.

(c) Sample 3.

(d) Sample 4.

Figure 20: Comparison of the effects of source SPL on LEONAR samples with different tube lengths.

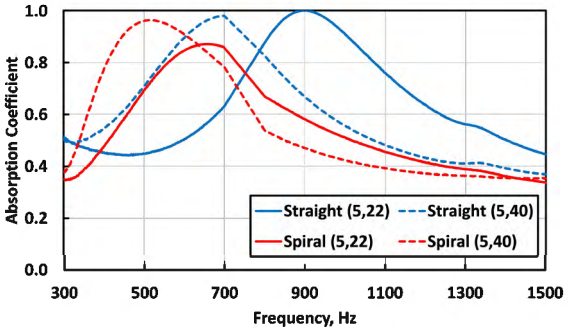

(a) Absorption coefficient.

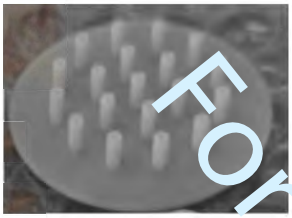

(b) Straight tubes; 0.5 mm radius, 22 or 40 mm insertion.

(c) Spiral tubes; 0.5 mm radius, 22 or 40 mm insertion.

Figure 21: Comparison of straight and spiral tube LEONAR liners.

2. *Piled 2DOF LEONAR*

The behavior of piled 2DOF resonators, where tubes protrude downward from both the facesheet and the septum, is relatively well understood to provide sound absorption in two distinct frequency ranges. Further advantages can be achieved by allowing the lower tubes (shown in green in Fig. 22) to also protrude into the upper cavity.

Figure 23 provides absorption coefficient spectra for two piled 2DOF resonators, each with a cavity thickness of 39 mm. Each liner contains 10 mm and 20 mm tubes, with orientations as shown. Although the thickness of each layer of the resonator remains unchanged, resonators with short top tubes and long bottom tubes (red curves) are demonstrated to provide a second frequency range with a high absorption. If the bottom cavity thickness is increased, this phenomenon is amplified, but it also generates a shift of the total absorption frequency band toward low frequencies. Since the piled 2DOF resonator (see Fig. 23(b)) supports long bottom tube lengths for a shallow lower cavity, absorption at low frequency bands can increase without this shift toward lower frequencies.[72]

A remarkable feature of 2DOF LEONAR liners for which the lower tubes protrude into both the upper and lower cavities is the possibility to maintain the absorption provided by a conventional SDOF liner while also achieving improved absorption over a second frequency band without altering the cavity thickness. This has to be contrasted with classical SDOF/2DOF resonators, for which the cavity thicknesses will need to

vary to achieve similar absorption spectra.

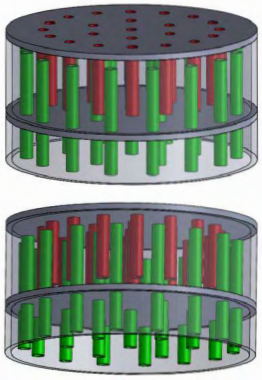

Figure 22: Piled LEONAR liner configurations.

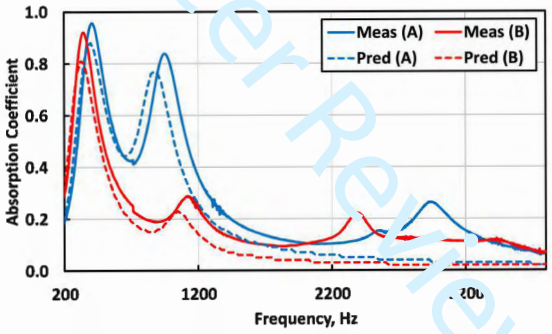

(a) Absorption coefficient.

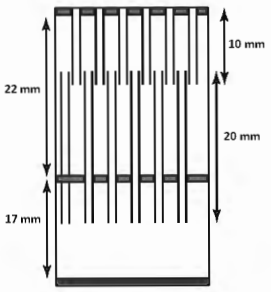

(b) Configuration A.

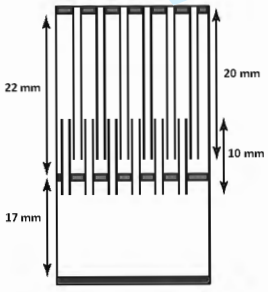

(c) Configuration B.

Figure 23: Comparison of two piled 2DOF resonator configurations.

3. *Parallel MDOF LEONAR*

The simplicity of LEONAR behavior may foster the optimization of MDOF resonators with parallel-impedance liners given, for example, by different tube lengths separated by partitions (see Fig. 24).[18, 71] The view of these liners is into the core from the backplate, where the facesheet containing the tubes is away from the reader. Figure 24(a) presents a 1D configuration that is subdivided into 90 chambers. The chambers in each ring have different shapes, and the tubes penetrating into each chamber may vary in length. On the other hand, the tube radius and POA remain identical for all of the chambers. The configuration depicted in Figure 24(b) is labeled as 3D because the sound field is assumed to (1) enter through the tube (appears as a white circle in the sketch) into the chamber (a total of 7 chambers for this configuration) and (2) change direction and propagate through the chamber that is parallel to the surface of the liner. Each of these samples has a diameter of 98 mm.

Overall, the arrangement of parallel cells should be macroscopically homogeneous, to avoid impedance discontinuities. However, one must define the ratio of each cell type surface area relative to the total area. Figure 25 shows the experimental and simulated absorption coefficient for a sample assumed to be a "metamaterial" in a large frequency range, because of a parallel distribution of 9 different tube lengths separated by partitions above 20 mm thick cavities. The curves are relatively similar except in the high frequency range for which the sensitivity is higher (for small tube lengths).

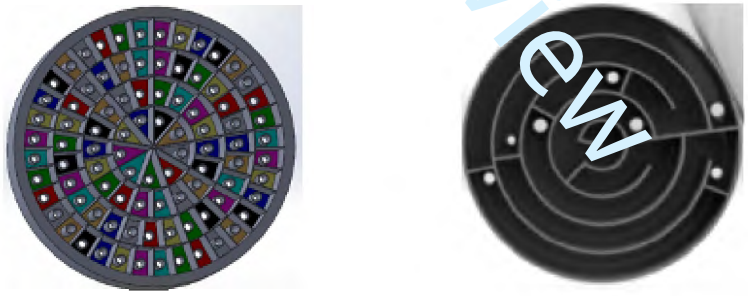

(a) 1D configuration. (b) 3D configuration.

Figure 24: Parallel MDOF LEONAR liner configurations. (a) 1D - tubes extend into core; (b) 3D - tubes extend into core and then into transverse plane.

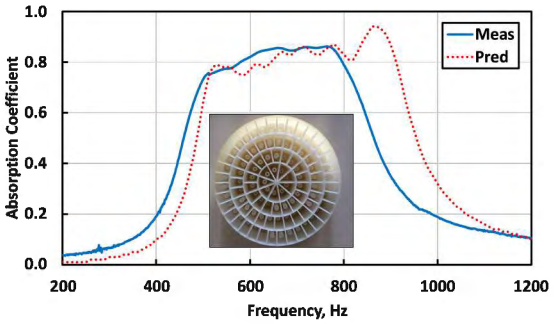

Figure 25: Comparison of measured and predicted absorption coefficient spectra for a parallel MDOF LEONAR liner.

Li and Assouar[73] have also introduced the concept of coils within the cavity space (see Fig. 24(b)). The idea is to increase the cavity length by distributing its length in a coplanar chamber, coiled around itself. This allows a drastic reduction of the resonance frequency but the challenge is to predict the actual "length" of the cavity seen by the wave. In addition, the perforations are replaced by tubes of various lengths, similar to a conventional LEONAR design. Figure 26 shows an example of an experimental absorption coefficient provided by a labyrinth metasurface based on a LEONAR design (with extended tubes) whose thickness is 20 mm. The sample achieves significant low frequency absorption in spite of its small thickness. Moreover, it highlights the fact that the incident SPL level has minimal influence on the absorption coefficient. Nevertheless, the band of peak attenuation is narrower than predicted by an analytical model (not shown).

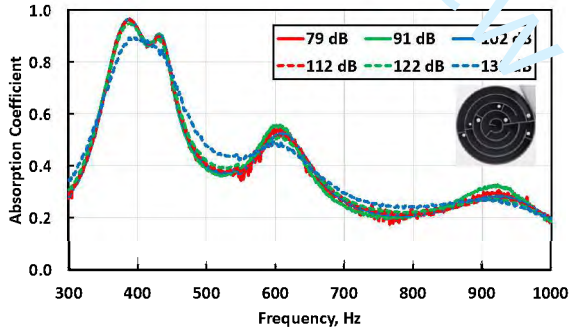

Figure 26: Effects of incident SPL on the absorption coefficient of a labyrinth metasurface based on a LEONAR design.

VII. Comparison Metrics

A. Overview

As mentioned earlier, the goal of any acoustic liner is to achieve increased acoustic performance relative to conventional liners while satisfying all of the airworthiness constraints, and to do so with a decrease (or at worst, no change) in liner drag. These goals are often addressed in a sequential manner. First, the designer seeks to find a liner concept that will satisfy a specific acoustic need. For example, there is a recent push to develop liners that maintain a reasonable amount of broadband absorption but also achieve good absorption at a specified lower frequency (e.g., at BPF). Next, the designer may seek to adjust the liner geometry such that the amount of drag produced by the liner is reduced. Finally, the last hurdle is to ensure that the concept can be manufactured to become flightworthy using cost-effective materials and manufacturing processes.

It is clearly important for the designer to have this last goal in mind from the outset. However, if good sound absorption and reduced liner drag are achieved, the likelihood of manufacturers developing cost-effective ways in which to build the liner is greatly enhanced. Novel liners often push the limits of manufacturability. The complexity of the design clearly affects the costs of manufacturing. For example, many concepts currently depend on additive manufacturing. This is very convenient for concept evaluation, but can be limiting for flightworthy applications. The materials used to manufacture the liner must be durable and load bearing, and have equal or less weight than current liners. Acoustic liners are expected to have a useful lifetime of at least twenty years. If they are mounted in the walls of the nacelle (typical location), they must have sufficient strength to support a technician standing on their surface to perform engine maintenance. For liners mounted in other portions of the aircraft, this load-bearing requirement may be less critical.

Acoustic liners are typically exposed to a very harsh environment. They are regularly exposed to high speed grazing flow, strong temperature shifts (hot in the desert, cold in flight), water (rainfall), jet fuel, sand, and dust. It is therefore imperitive that flightworthy liners be constructed with nonflammable materials, yet also be able to withstand numerous cycles of freezing and thawing of water without degradation. In addition to the thermal swings encountered throughout the flight cycle, some liners experience even higher temperatures. For example, liners mounted on the inner wall of the aft bypass duct, or within the walls of the engine core, must be constructed with materials capable of operation at high temperatures. In addition, the bonding material (glue) used to hold the liner components together must be able to handle these temperatures.

B. Aeroacoustic Metrics for Acoustic Liners

Each of the novel liner concepts presented in this paper are in early stages of development, and have been fabricated using additive manufacturing for ease of investigation in the NASA and ONERA test facilities. Thus, the aeroacoustic metrics presented here are related to two goals, namely acoustic absorption and liner drag reduction.

Tonal noise reduction

Depending on how the aircraft engine is designed, it is generally beneficial to absorb tones generated by the fan at BPF and/or 2BPF. Most of the configurations presented in this paper targeted BPF for tonal noise reduction, and also targeted a broadband noise reduction. It should be noted that most of these liner concepts could have targeted 2BPF just as easily. Indeed, the 2BPF tone is generally easier to attenuate than the BPF tone, as it occurs at a higher frequency. This metric is intended to account for engines where the BPF occurs at moderate frequencies, arbitrarily chosen to be at or above 1000 Hz.

Low frequency noise reduction

A significant byproduct of the increase in engine (and fan) diameter is the shift of BPF to lower frequencies (taken to be less than 1000 Hz for the purposes of this study). It is therefore becoming important for the liner to achieve tonal absorption at these lower frequencies. This is treated as a separate metric because the adaptation to handle lower frequencies may be noticeably different from that used for typical tonal noise reduction. For example, if a liner consisting of quarter-wavelength resonators is used, the chambers of the liner must be much longer to achieve absorption at these lower frequencies.

Broadband noise reduction

As the bypass ratio and engine diameter increase, the dominant noise transitions from tone-dominated to broadband. Thus, liners are needed to provide sound absorption over a wide range of frequencies. It is not enough to simply broaden the frequency range over which sound absorption occurs, but it is also important that the sound absorption is sufficiently high, i.e., high absorption coefficient or high attenuation for normal incidence and grazing incidence sound fields, respectively. Chambers et al.[4] presents a metric labeled the LFP (low-frequency performance) to capture low frequency and broadband performance for a normal incidence sound field, given by

$$\mathrm{LFP} = \frac{\beta_f M_p}{\beta_1} \times 100. \tag{31}$$

where β_f is the lowest continuous frequency bandwidth where the absorption coefficient is greater than a selected threshold (they chose 0.6 for their study), M_p is the maximum peak value of the absorption coefficient within the bandwidth, and β_1 is the lower bound of the bandwidth, β_f (note: variable names changed to avoid conflicts with current paper). Future studies of the current liners should be evaluated on this basis.

Predictability

Many semi-empirical models[1,38,40,48–50,74–80] have been developed over the years for conventional liners. These models enable the liner designer to accurately achieve target impedance spectra. It is critical that current models are adapted, or new models are developed, to accommodate novel liner configurations.[40] It is also important to note that each of these models were developed with a particular application in mind. Some were designed for no-flow, normal incidence applications, while others were developed for use in aircraft engine nacelles with high speed grazing flows. As noted earlier, much of the initial liner concept evaluation occurs in the no-flow, normal incident environment, as this is much less expensive and therefore allows exploration of many different liner configurations. However, if these liners are to eventually make their way into aircraft engine nacelles, their acoustic performance must also be predictable in that environment.

Linearity

Acoustic liners with conventional perforate facesheets are known to be weakly nonlinear, i.e., their surface impedance is sensitive to changes in the acoustic particle velocity (and therefore, the SPL) that impinges on the liner surface (recall the results of Fig. 17 for a conventional liner). If nonlinearity effects are well understood, they can be used as another control mechanism to achieve a desired impedance. However, many liner designers prefer to design the liner to be more linear (insensitive to changes in the incident acoustic particle velocity or SPL), as this type of liner is usually also insensitive to changes in the velocity of mean flow over the liner surface. This simplifies the design process, as simple tests in a no-flow environment can be used to predict the acoustic performance in a more complex grazing flow environment. For the purposes of this review, we will define increased linearity as a measure of goodness.

Liner drag

The rough surface and air jetting through the surface of the perforated facesheet cause the drag to be increased relative to a smooth surface. Reductions in this liner drag enable reductions in fuel, and are therefore very desirable. Based on input from aircraft engine companies, NASA has established a goal of 80% reduction in drag caused by acoustic liners relative to the amount of drag produced by current conventional

liners. Although this goal is quite aggressive, recent results[32, 33] suggest that it is not unreasonable. As novel liners are considered for use in locations other than the nacelle, this becomes even more critical. The extraordinary attention to fuel consumption in the current marketplace requires that acoustic performance be sufficiently large to offset any aerodynamic penalties (e.g., liner drag) caused by the introduction of acoustic liners in unconventional locations.

C. Comparison of Current Liners

Table 1 provides a listing of the concepts (both conventional and novel) discussed in this paper and Table 2 presents an attempt by the authors to quantify the relative merits of each liner concept based on the aeroacoustic metrics discussed above. For each metric, scores from 1 to 5 are used to indicate a range of performance from poor to excellent.

Table 1: List of liner concepts.

Concept	**Label**	**Concept**	**Label**
1	Conventional SDOF	5	Shared inlet port
2	MDOF with embedded mesh caps	6a	SDOF LEONAR (cross/star)
3a	Variable-depth (straight, no facesheet)	6b	SDOF LEONAR (straight)
3b	Variable-depth (bent, no facesheet)	6c	SDOF LEONAR (spiral)
3c	Variable-depth (straight, with facesheet)	7	Piled 2DOF LEONAR
4a	Variable facesheet (120 dB source)	8	Parallel 1D MDOF LEONAR
4b	Variable facesheet (140 dB source)	9	Parallel 3D MDOF LEONAR

Table 2: Aeroacoustic comparison metrics (1=poor, ..., 5=excellent).

	Liner Concept								
Metric	**1**	**2**	**3**	**4**	**5**	**6**	**7**	**8**	**9**
Tonal noise reduction	5	4	4	3	4	3	4	4	4
Low frequency noise reduction	1	2	4	2	4	5	5	5	5
Broadband noise reduction	3	5	5	4	4	3	4	5	4
Predictability	4	3	3	3	3	4	4	3	2
Linearity	2	3	2	2	3	4	4	4	4
Liner drag	2	2	3	3	5	2	2	2	2

The scores presented in Table 2 suggest that the NASA configurations (1 - 5) are preferred for broadband noise reduction, while the ONERA configurations (concepts 6 - 9) are preferred for low frequency noise reduction. A few of the NASA concepts score higher for the liner drag metrix (i.e., they produce less drag),

while the ONERA concepts tend to be more linear. However, it is important to note that these scores are based on the particular configurations of each concept that were considered in this study. Therefore, it is quite possible that these results will vary depending on the way in which a concept is to be used.

These scores represent the current thinking of the authors, and are expected to be modified as more rigorous quantification metrics are established and more evaluation tests are conducted. Regardless, this scoring system is intended to provide an initial estimate as to where each liner concept currently resides, and where there is room for improvement. It is noted that the authors feel that further work is needed regarding predictability for all of the concepts presented here. Also, the linearity scores of the current concepts are all between 2 and 4. This is intentional, to allow for other liners with more or less linearity to be added to this comparison.

Finally, Figure 27 provides an overview of the acoustic absorption achieved with each of the liner concepts included in this study. The abscissa represents the lower bound of the frequency range for which the absorption coefficient is expected to be at least 0.6, while the ordinate indicates the frequency range over which this absorption occurs. Note that some of the concepts appear at more than one location on the graph, indicating multiple frequency ranges for which the absorption is high. As an example, concept 6b (SDOF LEONAR with straight tubes) provides good sound absorption for a 510 Hz frequency bandwidth with a lower bound of 440 Hz (i.e., from 440 to 950 Hz), and also provides good sound absorption for a 560 Hz frequency bandwidth with a lower bound of 680 Hz (i.e., from 680 to 1240 Hz). The blue and green hemispheres depict the frequency regimes targeted by the ONERA and NASA concepts, respectively. This graphic clearly demonstrates that the ONERA concepts included in this study tend to focus on low frequency absorption, whereas the NASA concepts target broadband absorption.

VIII. Concluding Remarks

This paper has presented a number of novel liner concepts developed over the last few decades by NASA and more recently (during the last decade) by ONERA. Each concept developed by NASA is designed to vary the impedance over the liner surface. These include variable-depth (with straight or bent chambers), variable facesheet, and shared inlet port configurations. The concepts developed by ONERA are based on the LEONAR (Long Elastic Open Neck Acoustic Resonator) design, and include SDOF LEONAR liners with variable tube shapes, piled 2DOF LEONAR liners, and parallel MDOF liners. A brief review was provided regarding conventional liners currently employed in commercial aircraft engine nacelles, along with a review of each of the aforementioned novel liner concepts. Impedance prediction models used in the design

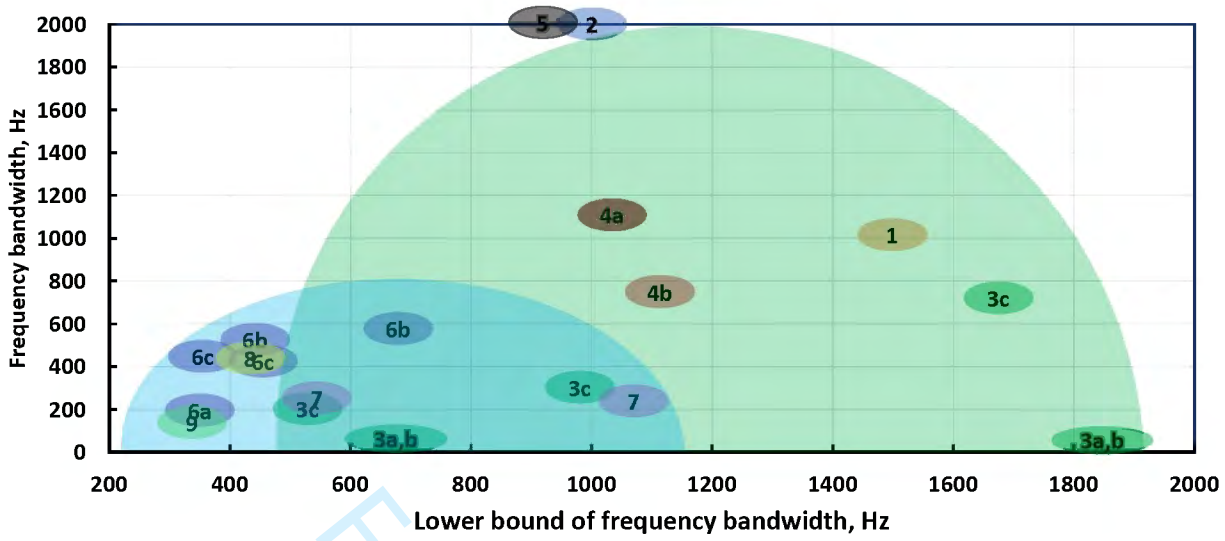

Figure 27: Comparison of liner concepts - target $\alpha > 0.6$. Labels correspond to Table 1. Blue and green hemispheres represent frequency domains of interest for NASA and ONERA concepts, respectively.

of these liner concepts were discussed, and selected results were presented for each of these liners. Finally, a set of aeroacoustic metrics was proposed for comparison of acoustic liners, and each of these concepts was compared on this basis.

Acknowledgments

The first author would like to acknowledge funding support provided by the Advanced Air Transport Technology Project of the NASA Advanced Air Vehicles Program, and the contributions of Douglas Nark, Brian Howerton, Noah Schiller, Martha Brown, and Alonso (Max) Reid of the NASA Langley Liner Physics Team regarding investigations of the NASA liner concepts. The second and third authors would like to acknowledge funding support provided by ONERA, and the help of Delphine Sebbane for the acoustic sample preparation.

References

[1]Ingard, U., "On the Theory and Design of Acoustic Resonators," *Journal of the Acoustical Society of America*, Vol. 25, 1953, pp. 1037–1061, doi:10.1121/1.1907235.

[2]"URL://www.acare4europe.org/documents/strategic-research-innovation-agenda-2017-update," [cited 1 February 2021] "Strategic Research and Innovation Agenda - 2017 update Vol 1", Advisory Council for Aviation Research and Innovation in Europe, 2017.

[3]de la Riva, D., Burdisso, R., and Ng, W., "AFT fan noise control using Herschel-Quincke/liner system," AIAA Paper 2005-3071, 2005, doi:10.2514/6.2005-3071.

[4]Chambers, A., Manimala, J. M., and Jones, M. G., "Improved Low-Frequency Broadband Absorption using 3D Folded Cavity Acoustic Liners," to appear in the proceedings of the Institute of Noise Control Engineering NoiseCon17 Congress and Conference, Grand Rapids, MI, June, 2017. 1, June 2017.

[5]Watson, W., Robinson, J., Jones, M., and Parrott, T., "Computational Study of Optimum and Off-design Performance of Checkerboard Liners," AIAA Paper 2004-3030, May 2004, doi:10.2514/6.2004-3030.

[6]Beck, B. S., Schiller, N. H., and Jones, M. G., "Impedance assessment of a dual-resonance acoustic liner," *Applied Acoustics Journal*, Vol. 93, June 2015, pp. 15–22, doi:10.1016/j.apacoust.2015.01.011.

[7]Bake, F. and Knobloch, K., "Novel liner concepts," *CEAS Aeronautical Journal*, March 2019, pp. 123–136, doi:10.1007/s13272-019-00380-7.

[8]Bielak, G. W., Premo, J. W., and Hersh, A. S., "Advanced Turbofan Duct Liner Concepts," NASA CR 209002, 1999.

[9]Williams, K., Chiu, G., and Bernhard, R., "Adaptive-Passive Absorbers Using Shape-Memory Alloys," *Journal of Sound and Vibration*, Vol. 249, No. 5, 2002, pp. 835–848, doi:10.1006/jsvi.2000.3496.

[10]Liu, F., Horowitz, S., Nishida, T., Cattafesta, L., and Sheplak, M., "A Tunable Electromechanical Helmholtz Resonator," AIAA Paper 2003-3145, 2003.

[11]Ichihashi, F., "Structure with Active Acoustic Openings," U.S. Patent 2013/0341119 A1, Dec. 2013.

[12]Jones, M. G., Parrott, T. L., Heidelberg, L. J., and Envia, E., "Low-Noise Fan Exit Guide Vanes," U.S. Patent 7334998, February 2008.

[13]Jones, M. G., Parrott, T. L., Sutliff, D. L., and Hughes, C. E., "Assessment of Soft Vane and Metal Foam Engine Noise Reduction Concepts," AIAA Paper 2009-3142, May 2009.

[14]Jones, M., Khorrami, M., Choudhari, M., and Howerton, B., "Flap Side Edge Liners for Airframe Noise Reduction," U.S. Patent 8695915, April 2014.

[15]Jones, M. G. and Howerton, B. M., "Evaluation of Novel Liner Concepts for Fan and Airframe Noise Reduction," AIAA Paper 2016-2787, May 2016.

[16]Mery, F., Piot, E., Sebbane, D., Reulet, P., Simon, F., and Mendez, A. C., "Experimental assessment of the effect of temperature gradient across an aeroacoustic liner," *Journal of Aircraft*, Vol. 56, No. 5, May 2019, doi:10.2514/1.C035157.

[17]Simon, F., Ghouali, A., Fascio, V., and Fleury, V., "Development and assessment of a low frequency acoustic liner design for landing systems noise minimization," *Journal of the Acoustical Society of America, Proceedings of Meetings on Acoustics*, Vol. 42, 065001, 2021, doi:10.1121/1.5147051.

[18]Simon, F., Mery, F., Roncen, R., Sebbane, D., and Piot, E., "Inlet Liner Design for aircraft air conditioning system," June 2019, Inter-Noise 2019.

[19]Ma, X. and Su, Z., "Development of acoustic liner in aero engine: A review," *Science China Technological Sciences*, Vol. 63, No. 12, Aug. 2020, doi:10.1007/s11431-019-1501-3.

[20]Marinova, M. M., Jones, M. G., and Schiller, N. H., "Evaluation of Packing3D Code for Design of Variable-Depth, Bent-Chamber Acoustic Liners," NASA TM 220560, February 2020.

[21]Simon, F., Marchner, P., Romcen, R., and Chevillotte, F., "Comportement d'un liner acoustique par approche de type Lattice Boltzmann," Cfa 2018 - le havre, April 2018.

[22]Howerton, B. M., Jones, M. G., and Jasinski, C. M., "Acoustic Liner Drag: Further Measurements on Novel Facesheet Perforate Geometries," AIAA Paper 2018-3605, June 2018.

[23]Blackstock, D. T., *Fundamentals of Physical Acoustics*, Wiley, doi:10.1121/1.1354982, 2000.

[24]Ayle, E., "Acoustic Septum Honeycomb," U.S. Patent 2011/0073407A1, March 2011, No DOI found.

[25]Jones, M. G., Howerton, B. M., and Ayle, E., "Evaluation of Parallel-Element, Variable-Impedance, Broadband Acoustic Liner Concepts," AIAA Paper 2012-2194, June 2012.

[26]Nark, D. M. and Jones, M. G., "Broadband Liner Optimization for the Source Diagnostic Test Fan," AIAA Paper 2012-2195, June 2012.

[27]Nark, D. M., Jones, M. G., and Sutliff, D. L., "Further Development and Assessment of a Broadband Liner Optimization Process," AIAA Paper 2016-2784, May 2016.

[28]Jones, M. G., Nark, D. M., Baca, A., and Smith, C. R., "Applications of Parallel-Element, Embedded Mesh-Cap, Acoustic Liner Concepts," AIAA Paper 2018-3445, June 2018.

[29]Nark, D. M., Jones, M. G., Schiller, N. H., and Sutliff, D. L., "Broadband Inlet Liner Design for the DGEN Aeropropulsion Research Turbofan," AIAA Paper 2018-3608, June 2018.

[30]Sutliff, D. L., Nark, D. M., Jones, M. G., and Schiller, N. H., "Design and Acoustic Efficacy of a Broadband Liner for the Inlet of the DGEN Aero-propulsion Research Turbofan," AIAA Paper 2019-2582, May 2019.

[31]"URL: https://www.nasa.gov/pdf/458490main_TRL_Definitions.pdf," [cited 29 June 2020].

[32]Nark, D. M. and Jones, M. G., "Design of an Advanced Inlet Liner for the Quiet Technology Demonstrator 3," AIAA Paper 2019-2764, May 2019.

[33]Wong, J. W., Nesbitt, E. H., Jones, M. G., and Nark, D. M., "Flight Test Methodology for NASA Advanced Inlet Liner on 737MAX-7 Test Bed (Quiet Technology Demonstrator 3)," AIAA Paper 2019-2763, May 2019.

[34]Cummer, S., Christensen, J., and Alu, A., "Controlling sound with acoustic metamaterials," *Nature Reviews Materials*, Vol. 16001, No. 1, Feb. 2016, doi:10.1038/natrevmats.2016.1.

[35]Howerton, B. M. and Jones, M. G., "Acoustic Liner Drag: A Parametric Study of Conventional Configurations," AIAA Paper 2015-2230, June 2015.

[36]Gerhold, C. H., Brown, M. C., and Jasinski, C. M., "Evaluation of Skin Friction Drag for Liner Applications in Aircraft," AIAA Paper 2016-1267, January 2016.

[37]Howerton, B. M. and Jones, M. G., "A Conventional Liner Acoustic/Drag Interaction Benchmark Database," AIAA Paper 2017-4190, June 2017.

[38]Parrott, T. L. and Jones, M. G., "Parallel-Element Liner Impedances for Improved Absorption of Broadband Sound in Ducts," *Noise Control Engineering Journal*, Vol. 43, No. 6, Nov. 1995.

[39]Tijdeman, H., "On the propagation of sound waves in cylindrical tubes," *Journal of Sound and Vibration*, Vol. 39, No. 1, 1975, pp. 1–33.

[40]Zwikker, C. and Kosten, C., *Sound absorbing materials*, Elsevier Publishing Company, 1949.

[41]Jones, M. G., Watson, W. R., Nark, D. M., Schiller, N. H., and Born, J. C., "Optimization of Variable-Depth Liner Configurations for Increased Broadband Noise Reduction," AIAA Paper 2016-2783, May 2016.

[42]Allard, J. F. and Atalla, N., "Propagation of Sound in Porous Media," oct 2009, doi:10.1002/9780470747339.

[43]Johnson, D. L., Koplik, J., and Dashen, R., "Theory of dynamic permeability and tortuosity in fluid-saturated porous media," *Journal of Fluid Mechanics*, Vol. 176, 1987, pp. 379–402, doi:10.1017/s0022112087000727.

[44]Champoux, Y. and Allard, J.-F., "Dynamic tortuosity and bulk modulus in air-saturated porous media," *Journal of Applied Physics*, Vol. 70, No. 4, 1991, pp. 1975–1979, doi:10.1063/1.349482.

[45]Pride, S. R., Morgan, F., and Gangi, A. F., "Drag forces of porous-medium acoustics," *Physcis Review B*, Vol. 47, No. 9, 1993, pp. 4964–4978.

[46]Lafarge, D., Lemarinier, P., Allard, J. F., and Tarnow, V., "Dynamic compressibility of air in porous structures at audible frequencies," *Journal of the Acoustical Society of America*, Vol. 102, No. 4, Oct. 1997, pp. 1995–2006, doi:10.1121/1.419690.

[47]Atalla, N. and Sgard, F., "Modeling of perforated plates and screens using rigid frame porous models," *Journal of Sound and Vibration*, Vol. 303, No. 1-2, 2007, pp. 195–208, doi:10.1016/j.jsv.2007.01.012.

[48]Motsinger, R. E. and Kraft, R. E., "Design and Performance of Duct Acoustic Treatment: Aeroacoustics of Flight Vehicles; Chapter 14, Vol. 2: Noise Control," NASA RP 1258, Aug. 1991.

[49]Parrott, T. L. and Jones, M. G., "Assessment of NASA's Aircraft Noise Prediction Capability, Chapter 6: Uncertainty in Acoustic Liner Impedance Measurement and Prediction," NASA TP 2012-215653, July 2012.

[50]Rice, E. J., "A Model for the Acoustic Impedance of a Perforated Plate Liner With Multiple Frequency Excitation," NASA TP 1613, 1980.

[51]Heidelberg, L. J., Rice, E. J., and Homyak, L., "Experimental Evaluation of a Spinning-Mode Acoustic-Treatment Design Concept for Aircraft Inlets," NASA TP 1613, April 1980.

[52]Howerton, B. M., Vold, H., and Jones, M. G., "Application of Sine Sweep Excitation for Acoustic Impedance Eduction," AIAA Paper 2019-2487, May 2019.

[53]Jones, M. G. and Parrott, T. L., "Evaluation of a multi-point method for determining acoustic impedance," *Journal of Mechanical Systems and Signal Processing*, Vol. 3, No. 1, 1989, pp. 15–35.

[54]Jones, M. G. and Stiede, P. E., "Comparison of Methods for Determining Specific Acoustic Impedance," *Journal of the Acoustical Society of America*, Vol. 101, No. 5, May 1997, pp. 2694–2704.

[55]ASTM E1050-19, "Standard Test Method for Impedance and Absorption of Acoustical Materials Using a Tube, Two Microphones, and a Digital Frequency Analysis System," ASTM International, West Conshohocken, PA, 2019, No DOI found.

[56]Chung, J. Y. and Blaser, D. A., "Transfer function method of measuring in-duct acoustic properties: I. Theory," *Journal of Acoustical Society of America*, Vol. 68, 1980, pp. 907–921, doi:10.1121/1.384778.

[57]Cummings, A., "Sound Transmission in Curved Duct Bends," *Journal of Sound and Vibration*, Vol. 35, No. 4, 1974, pp. 451–477.

[58]"COMSOL Acoustic Module User's Guide," v5.1, 2015.

[59]Jones, M. G., Nark, D. M., Watson, W. R., and Howerton, B. M., "Variable-Depth Liner Evaluation Using Two NASA Flow Ducts," AIAA Paper 2017-3022, June 2017.

[60]Jones, M., Watson, W., Nark, D., and Schiller, N., "Evaluation of Spanwise Variable Impedance Liners with Three-Dimensional Aeroacoustics Propagation Codes," AIAA Paper 2017-3021, June 2017, doi:10.2514/6.2017-3021.

[61]Schiller, N. H., Jones, M. G., Howerton, B. M., and Nark, D. M., "Developments of a Low-Drag Variable-Depth Acoustic Liner," AIAA Paper 2019-2749, May 2019.

[62]Brown, M. C. and Jones, M. G., "Evaluation of Variable Facesheet Liner Configurations for Broadband Noise Reduction," AIAA Paper 2020-2616, June 2020, doi:10.2514/6.2020-2616.

[63]Brown, M. C. and Jones, M. G., "Evaluation of a Variable Facesheet Liner Configuration in Grazing Incidence Flow," AIAA Paper 2021-2243, Aug. 2021.

[64]Simon, F., "Long Elastic Open Neck Acoustic Resonator for Low Frequency Absorption," *Journal of Sound and Vibration*, Vol. 421, 2018, pp. 1–16, doi:10.1016/j.jsv.2018.01.044.

[65]Zhao, H., Lu, Z., Guan, Y., Li, G., Liu, J., and Ji, C., "Effect of extended necks on transmission loss performances of Helmholtz resonators in presence of a grazing flow," *Aerospace Science and Technology*, Vol. 77, 2018, pp. 228–234, doi:10.1016/j.ast.2018.03.002.

[66]Roncen, R., Sebbane, D., Mery, F., Piot, E., and Simon, F., "Experimental Investigation of Shear Grazing Flow Effects on Extended Tube Acoustic Liners," eforum acusticum, Dec. 2020, doi:10.48465/fa.2020.0225.

[67]Yang, C. and Zhang, P., "Investigation of Extended-Tube Liners for Control of Low-Frequency Duct Noise," *AIAA Journal*, 2021, pp. 1–16, doi:10.2514/1.j059988.

[68]Simon, F., "Low frequency sound absorption of resonators with flexible tubes," 2013, Proceedings for the International Congress of Acoustics.

[69]Ingard, U. and Labate, S., "Acoustic Circulation Effects and the Nonlinear Impedance of Orifices," *Journal of the Acoustical Society of America*, Vol. 22, 1950, pp. 211–218, doi:10.1121/1.1906591.

[70]Simon, F., "Garniture Surfacique pour Absorption Acoustique," INPI Patent 3,065,570, May 2019.

[71]Simon, F., Mery, F., Roncen, R., Sebbane, D., Piot, E., Davoine, C., and Thomas, M., "Overview of low frequency resonators based on LEONAR design," 2020, Noise-Con 2020.

[72]Simon, F. and Sebbane, D., "Compact 2DOF Liner Based On A Longe Elastic Open Neck Acoustic Resonator For Low Frequency Absorption," *Noise Control Engineering Journal*, Vol. 69, No. 1, Jan. 2021, pp. 1–17, doi:10.3397/1/37691.

[73]Li, Y. and Assouar, B., "Acoustic metasurface-based perfect absorber with deep subwavelength thickness," 2016, doi:10.1063/1.4941338, Applied Physics Letters 108, No. 6.

[74]Melling, T. H., "The Acoustic Impedance of Perforates at Medium and High Sound Pressure Levels," *Journal of Sound and Vibration*, Vol. 29, No. 1, 1973, pp. 1–65.

[75]Guess, A. W., "Calculation of perforated plate liner parameters from specified acoustic resistance and reactance," *Journal of Sound and Vibration*, Vol. 40, No. 1, 1975, pp. 119–137, doi:10.1016/s0022-460x(75)80234-3.

[76]Maa, D., "Potential of microperforated panel absorber," *Journal of the Acoustical Society of America*, Vol. 104, No. 5, 1998, pp. 2861–2866.

[77]Betts, J. F., "Experiments and Impedance Modeling of Liners Including the Effect of Bias Flow," Ph.D. Dissertation, Virginia Tech, Blacksburg, VA, July 2000.

[78]Kabral, R., Bodén, H., and Elnady, T., "Determination of Liner Impedance under High Temperature and Grazing Flow Conditions," AIAA Paper 2003-3304, May 2003.

[79]Parrott, T. L. and Jones, M. G., "Cascaded Perforates as One-Dimensional, Bulk Absorbers," AIAA Paper 2006-2402, 2006.

[80]Yu, J., Ruiz, M., and Kwan, H. W., "Validation of Goodrich Perforate Liner Impedance Model Using NASA Langley Test Data," AIAA Paper 2008-2930, May 2008.